

THESIS FOR THE DEGREE OF LICENTIATE OF ENGINEERING

Hydromechanical Behaviour of Fractures Close to Tunnels
in Crystalline Rock

JOHAN THÖRN

Department of Civil and Environmental Engineering
Division of GeoEngineering
CHALMERS UNIVERSITY OF TECHNOLOGY
Gothenburg, Sweden 2013

Hydromechanical Behaviour of Fractures Close to Tunnels in Crystalline Rock

JOHAN THÖRN

© JOHAN THÖRN, 2013

Lic / Department of Civil and Environmental Engineering, Chalmers University of Technology.

lic 2013:5,
ISSN 1652-9146

Department of Civil and Environmental Engineering
Division of GeoEngineering
Chalmers University of Technology
SE-412 96 Gothenburg
Sweden
Telephone + 46 (0)31-772 1000

Chalmers Reproservice
Gothenburg, Sweden 2013

Hydromechanical Behaviour of Fractures Close to Tunnels in Crystalline Rock

JOHAN THÖRN

Department of Civil and Environmental Engineering

Division of GeoEngineering

Chalmers University of Technology

ABSTRACT

The deformation and stiffness properties of rock fractures are important measurable parameters when describing their hydromechanical behaviour. Deformation refers to aperture change. Stiffness refers to the amount of deformation per stress change to which a fracture is subjected. This thesis aims to investigate the stiffness and deformation behaviour of fractures in crystalline rock through in situ and laboratory experiments. The focus in this work is on fracture geometry due to geological stress history. This will result in increased conceptual understanding and accordance between hydromechanical and geomechanical fracture description and behaviour.

The in situ measurements consisted of deformation measurements in boreholes and were conducted at the Äspö Hard Rock Laboratory (HRL) and in the Hallandsås Tunnel. The total deformation across the instrumented borehole sections was measured as an effect of hydraulic pressurisation of the fractures in the nearby rock volume. The results were assessed in terms of deformation and fracture stiffness.

The laboratory experiments were conducted as cyclically loaded permeameter measurements of fractured rock core samples from Äspö HRL with simultaneous deformation measurements across the fracture. The tested samples had various geological properties and revealed differences in hydraulic aperture and mechanical deformation behaviour across the experimental cycles.

The stiffness to hydraulic aperture relationship followed a trend identified in the literature and deviations were given plausible explanations related to the geology and geometry of the samples. The results were discussed in the light of the sampled geology and the measurement methods. The measured deformations and corresponding stiffness were found to be reasonable in the light of available knowledge of the local geology and stress situation at the sites.

Keywords:

Hydromechanical coupling, Fracture stiffness, Deformation measurement, Äspö HRL, Hallandsås, Geological history, In situ, Laboratory experiments, Fracture geometry, Rock stress

Hydromekaniskt beteende hos sprickor nära tunnlar i kristallint berg

JOHAN THÖRN

Institutionen för bygg och miljöteknik

Avdelningen för geologi och geoteknik

Chalmers tekniska högskola

SAMMANDRAG

Deformationsegenskaper och sprickstyvhet är mätbara parametrar som är viktiga för att beskriva det hydromekaniska beteendet hos sprickor i berg. Deformation uttrycks som en viddändring hos en spricka. Styvhet avser mängden deformation per spänningsförändring som en spricka utsätts för. Denna uppsats syftar till att genom fält- och laboratorieexperiment undersöka styvhets- och deformationsbeteendet för sprickor i kristallint berg. Fokus ligger på sprickgeometri kopplat till den geologiska spänningshistorien och förhoppningen är att bidra till en ökad samsyn och konceptuell förståelse mellan hydromekanik och geomekanik.

Fältmätningarna bestod i deformationsmätningar i borrhål, som utfördes i Äspölaboratoriet och i Hallandsåstunneln. Den totala deformationen över en borrhålssektion mättes under tiden som den närliggande bergvolymen utsattes för injektion av vatten eller injekteringsbruk under förhöjt tryck. Resultaten utvärderades som sprickstyvhet.

Laboratorieexperimenten utfördes som cykliska permeameterförsök på spruckna kärnprover från Äspölaboratoriet samtidigt som deformationer över sprickan registrerades. Proverna hade olika geologiska egenskaper och uppvisade olika beteende med hänsyn till hydraulisk vidd och den upmätta mekaniska deformationen.

Förhållandet mellan styvhet och hydraulisk vidd följde ett samband som hämtats från litteraturen och avvikelser från denna förklarades utifrån ometriska egenskaperna hos de avvikande proverna. Resultaten diskuteras i termer av geologiska parametrar hos de undersökta bergvolymerna samt om mätmetoderna i sig. Uppmätta deformationer och motsvarande sprickstyvhet är rimliga om de sätts i ljuset av tillgänglig information kring geologin och bergspänningssituationen vid de provtagna platserna.

LIST OF PUBLICATIONS

This thesis includes the following publications, referred to by roman numerals in the text.

- I. Thörn J, Runslätt E, Fransson Å, Funehag J, Gustafson G (2012) Fracture Deformation Measurements during Grouting in Hard Rock. Paper presented at the *4th International Conference on grouting and Deep Mixing*, New Orleans, LA, USA.
- II. Fransson Å, Thörn J, Ericsson LO, Lönnqvist M, Stigsson M (2012) Hydromechanical characterization of fractures close to a tunnel opening: A case study. Paper presented at *Eurock2012*, Stockholm, Sweden.
- III. Thörn J, Ericsson LO, Fransson Å (2013) Hydraulic and Hydromechanical Laboratory Testing of Large Crystalline Rock Cores. Submitted to *Rock Mechanics and Rock Engineering*.

The following publications are not appended but were written within the framework of the project.

- IV. Thörn J, Fransson Å (2011) Skattning av sprickstyvhet baserat på hydrauliska tester och injekteringsdata. Paper presented at the *Bergmekanikdag 2011*, BeFo, Stockholm, Sweden.
Available at: <http://cpl.lib.chalmers.se/publication/138075>
- V. Thörn J (2012) *Coupling between changes in hydraulic and mechanical aperture: A laboratory study on rock cores*. Report / Department of Civil and Environmental Engineering, Chalmers University of Technology 2012:9. ISSN-1652-9162. Gothenburg, Sweden.
Available at: <http://cpl.lib.chalmers.se/publication/171899>

PREFACE

The work presented in this thesis was carried out at the Division of GeoEngineering, Chalmers University of Technology, and is the result of the first half of the PhD project entitled *Conceptual understanding of the rock mass hydromechanical properties*. The project was initiated and financed within the *Rock Mechanics Research Programme* at the Swedish Nuclear Fuel and Waste Management Co, SKB.

Sincere thanks to SKB for funding the project, for enabling experiments and sampling at Äspö HRL and for their feedback on the work. I would like to mention in particular Rolf Christiansson and Raymond Munier for their contribution to the latter. Thank you also to Skanska/Vinci and the Swedish Transport Administration for providing the site and the opportunity to conduct the Hallandsås experiments.

I would like to express my gratitude to the co-authors of the publications, in order of appearance: Edward Runslätt, Åsa Fransson, Johan Funehag, Gunnar Gustafson, Lars O Ericsson, Margareta Lönnqvist and Martin Stigsson.

I would like to thank my colleagues at the Division of GeoEngineering for their company and laughter during our coffee breaks. I am very grateful to technician Aaro Pirhonen and research engineer Peter Hedborg for helping me with the equipment. My heartfelt thanks to Professor Lars O Ericsson, co-supervisor, and Associate Professor Åsa Fransson, examiner and main supervisor, for all their support, patience and interesting discussions about the inner being of something as abstract as a void in the ground.

Life is not just work. Many thanks to my friends and family for helping me to remember that and for putting up with me. I'm already halfway through!

Finally, thank you Sara, you are the best person I know.

Johan Thörn
Gothenburg, April 2013

TABLE OF CONTENTS

ABSTRACT	iii
SAMMANDRAG	iv
LIST OF PUBLICATIONS	v
PREFACE	vii
TABLE OF CONTENTS	ix
LIST OF NOTATIONS.....	xi
1 INTRODUCTION	1
1.1 Aims	3
1.2 Outline of the thesis.....	3
2 LITERATURE REVIEW	7
2.1 Tectonic and regional geological evolution of the Fennoscandian Shield.....	7
2.2 Stress conditions.....	12
2.3 Geological and geometrical description of fractures.....	17
2.4 Mechanical description of fractures.....	23
2.5 Hydraulic description of fractures	26
2.6 Hydromechanical description of fractures.....	30
3 HYDROMECHANICAL EXPERIMENTS IN SITU (PUBLICATIONS I & II)	35
3.1 In situ experimental design.....	36
3.2 Results.....	39
3.3 Reliability of in situ methods and results.....	41
4 HYDROMECHANICAL EXPERIMENTS IN THE LABORATORY (PUBLICATION III)	43
4.1 Development of lab equipment	44
4.2 Results.....	45
4.3 Reliability of laboratory method and results.....	47
5 DISCUSSION	49
5.1 Geological history and resulting fracture geometry	49
5.2 Fracture geometry, present stresses and stress changes.....	51
6 CONCLUSIONS	57
6.1 Further work.....	58
REFERENCES.....	59
PUBLICATIONS	

LIST OF NOTATIONS

Roman Letters

a	[m]	Aperture
a	[m]	Radius of circular opening (Kirsch)
A	[m ²]	Cross section area
b	[m]	Hydraulic aperture
c	[-], [%]	Contact area between surfaces
c	[Pa]	Cohesion
C_f	[Pa ⁻¹]	Compressibility of fluid
D_f	[m]	Hydraulic diameter
dh	[m]	Pressure head change
d_{mob}	[°]	Mobilised dilation angle (Barton)
e	[m]	Hydraulic aperture (e.g. Barton)
e_v	[m]	Void aperture
E	[m]	Mechanical aperture (e.g. Barton)
g	[m/s ²]	Acceleration due to gravity
h_H	[m]	Hydraulic aperture in Zimmerman & Bodvarsson
JCS	[Pa]	Joint wall Compressive Strength
JRC	[-]	Joint Roughness Coefficient
K	[m/s]	Conductivity
k_n	[Pa/m]	Fracture normal stiffness
k_{n0}	[Pa/m]	Stiffness at zero intercept (Bandis-Barton)
k_n^a	[Pa/m]	Normal stiffness from mechanical deformation
k_n^b	[Pa/m]	Normal stiffness from changed hydraulic aperture
k_n^s	[Pa/m]	Normal stiffness from hydraulic aperture through storativity
k_s	[Pa/m]	Shear stiffnes
M	[-]	Damage coefficient (Barton)
p	[Pa]	Groundwater pressure
p	[Pa]	Pressure
Q	[m ³ /s]	Flow
r	[m]	Distance from centre of circular opening (Kirsch)
Re	[-]	Reynolds' number
u	[Pa]	Groundwater pressure
u_n	[m]	Normal closure
u_s	[m]	Shear deformation
z	[m]	Depth below ground surface

Greek Letters

α	[-]	Correction factor for effective stress in fractured rock
Δ	[-]	Prefix for indicating "change of"
δ	[m]	Normal closure (Bandis-Barton)
θ	[°]	Angle from vertical (Kirsch)

μ	[Pa·s]	Viscosity
v	[m/s]	Velocity of flow
ρ	[kg/m ³]	Density
σ	[Pa]	Stress
σ'	[Pa]	Effective stress
σ_1	[Pa]	Major principal stress
σ_2	[Pa]	Intermediate principal stress
σ_3	[Pa]	Minor principal stress
σ_c	[Pa]	Rock compressive strength
σ_H	[Pa]	Major horizontal stress component
σ_h	[Pa]	Minor horizontal stress component
σ_h^2	[m]	Standard deviation of h
σ_n	[Pa]	Normal stress
σ_{ni}'	[Pa]	Initial effective normal stress (Goodman)
σ_r	[Pa]	Radial stress (Kirsch)
σ_v	[Pa]	Vertical principal stress component
σ_x	[Pa]	Stress component (Kirsch)
σ_z	[Pa]	Stress component (Kirsch)
σ_θ	[Pa]	Tangential stress (Kirsch)
τ	[Pa]	Shear stress
τ	[Pa]	Shear strength
$\tau_{r\theta}$	[Pa]	Shear stress on element (Kirsch)
ϕ	[°]	Angle of internal friction
ϕ_b	[°]	Friction angle (Barton)

Abbreviations

BIPS	Borehole Image Processing System
EDZ	Excavation Damage Zone
Ga	Lat. Giga annum; billion years
HF	Hydraulic Fracturing
HM	Hydro-Mechanical
HRL	Hard Rock Laboratory
HTPF	Hydraulic Tests of Pre-existing Fractures
Ma	Lat. Mega annum; million years
SDM	Site Descriptive Modelling
SKB	Swedish Nuclear Fuel and Waste Management Co
TASX	Tunnel-ASpö-[unique identification letter]
THM	Termo-Hydro-Mechanical
WPT	Water Pressure Test

1 INTRODUCTION

In modern society, knowledge of underground construction is advancing. Examples can be found related to increased use of underground space to accommodate the infrastructure in growing cities, for more rapid transport between cities, or for handling hazardous waste, such as spent nuclear fuel. Common to these three examples is the construction of tunnels in rock.

The response of a rock mass to the impact of tunnel construction for example in terms of stress redistributions and changes in groundwater pressure has been the subject of research for a long time, see e.g. (Terzaghi 1936; Jaeger and Cook 1969; Olofsson 1991; Gustafson 2012).

However, demands relating to work safety and safety in the long term, as well as the amount of permissible water inflow into underground constructions, are becoming stricter. This is due to the use of underground facilities for more sensitive uses, where water inflow is detrimental to the use of the tunnel, and for environmental reasons, where inflow into a tunnel causes a reduction in groundwater levels in the surroundings, affecting the built and natural environment. In the case of a final repository for spent nuclear fuel, environmental concerns are paramount and the facility designed according to the Swedish KBS-3 system need to be safe for 100,000 years (SKB 2011). The repository needs to provide a safe working environment during the active decades of construction and deposition of the waste, as well as keeping the waste, placed in copper canisters, intact and in place until the radiation level of the waste is similar to that of uranium ore (SKB 2011).

Normal and shear deformations of fractures, triggered by e.g. changing fluid pressure, are examples of processes that may reduce the long-term safety of a repository. Consequently, a deeper understanding of these and other coupled hydraulic and mechanical rock fracture processes is beneficial.

The title of the thesis is **Hydromechanical behaviour of fractures close to tunnels in crystalline rock**. *Hydromechanical* is a term that refers to the processes and properties that link the hydraulic and mechanical properties of a fractured rock mass (Figure 1). Within this framework thermal processes are often included, sometimes also chemical and more rarely biological processes.

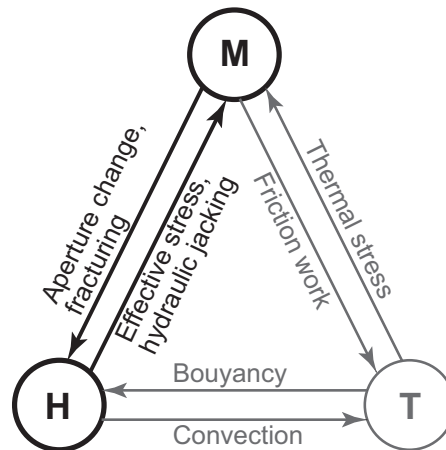


Figure 1: Termo-Hydro-Mechanical, THM-couplings for fractured rock. The HM couplings in focus in this work are highlighted. Adapted from Hökmark et al. (2006).

Fracture is by definition the common term for all types of mechanical breaks in rock (NRC 1996). In *crystalline rock*, which is the rock type commonly found in Sweden and the scope of this thesis, there are two main fracture types: joints and faults. A joint refers to a fracture that has been dilated in the normal direction to the fracture surfaces after the initial break of the rock (Mode I fracturing), while fault refers to a fracture that has undergone shearing, i.e. movement parallel to the fracture surfaces (Modes II or III).

With the key words in the title already defined briefly, some other brief definitions of key concepts for the thesis follow. The literature review chapter develop and deepen the description.

Aperture is a measure of the space between the surfaces of a fracture and is dependent on the *roughness* of the surfaces and the degree to which they fit to each other. The roughness is governed by the rock type, the type of fracture and the changes the fracture has undergone during and after it was originally formed.

An increased mechanical load across a fracture will cause a closure of the fracture, i.e. a reduction in the aperture. The amount of stress needed for unit deformation of a fracture is a characteristic of the fracture called stiffness. The stiffness is different in the normal direction (*normal stiffness*) and parallel to the fracture surface (*shear stiffness*) as well as for different stress situations. Large mechanical loads cause failure, i.e. fracturing of the rock. The *compressional strength*, i.e. the resistance of the rock to failure by compression, is significantly higher than the *tensional strength*, which is the rock's resistance to failure by dilation. The *stress field* redistributes around tunnels, which results in induced stresses of higher and lower intensity than the previous stress state. This influences fractures close to tunnels.

The volume used by the groundwater flow, the *hydraulic aperture*, is equal to or smaller than the average void between the fracture surfaces, the *mechanical aperture*. The ratio between hydraulic and mechanical aperture varies according to the type of fracture.

Effective stress refers to the rock stress minus groundwater pressure. If the groundwater pressure becomes higher than the rock stress the fractures will dilate substantially. This is termed *hydraulic jacking*.

1.1 Aims

The overall aim is the development of understanding and methodology for fracture geometry characterisation and description that results in increased accordance between hydromechanical and geomechanical fracture behaviour. The focus is on fracture geometry resulting from geological stress history.

The specific aims of this thesis are as follows:

- Analyse and predict the development of fracture stiffness and hydraulic aperture for fractures in crystalline rock.
- Contribute to increased understanding of how the actual aperture and contact geometry affect laboratory and in situ properties.
- Analyse and increase understanding of how parameters that are obtainable from in situ testing can characterise deformation properties and permeability.
- Describe the basic principles of how a fracture aperture distribution arises.
- Identify practical, in situ methods for evaluating fracture stiffness.

1.2 Outline of the thesis

The thesis is structured as follows: Chapter 2 contain a literature survey, where the focus is on geological, hydrogeological, rock mechanical and hydromechanical properties and processes within the boundary conditions of rock stresses. Relevant measurement methods are also briefly described. Suitable examples are taken from the sites of case studies in the appended publications: Äspö Hard Rock Laboratory (HRL) and the Hallandsås Tunnel project (see Figure 2).

Chapter 3 deals with hydromechanical experiments in situ, based on Publications I and II. Publication I describe deformation measurements performed in the wall of the Hallandsås Tunnel during a post-grouting campaign (PI in Figure 3). Publication II deals with characterisation of the TASSO Tunnel fracture system in Äspö HRL with deformation measurements performed in the floor of the tunnel (PII in Figure 3).

Chapter 4 deals with hydromechanical experiments in a laboratory environment and is based on Publication III, which describes cyclic permeameter tests with simultaneous deformation measurements. The laboratory experiments were conducted on samples drilled from slabs sawn out of the wall of the TASS and TASQ Tunnels at Äspö HRL (PIII in Figure 3). Chapters 3 and 4 also include a discussion of the experimental methods and means for improvement. In Chapter 5, the discussion includes the geology-related parameters as well as important differences between the sites.

The thesis concludes with a list of the main findings and a section on recommendations for further work on the topic.

Publications I-III are appended to the thesis and publications IV-V are available and freely accessible, e.g. in the Chalmers Publication Library.

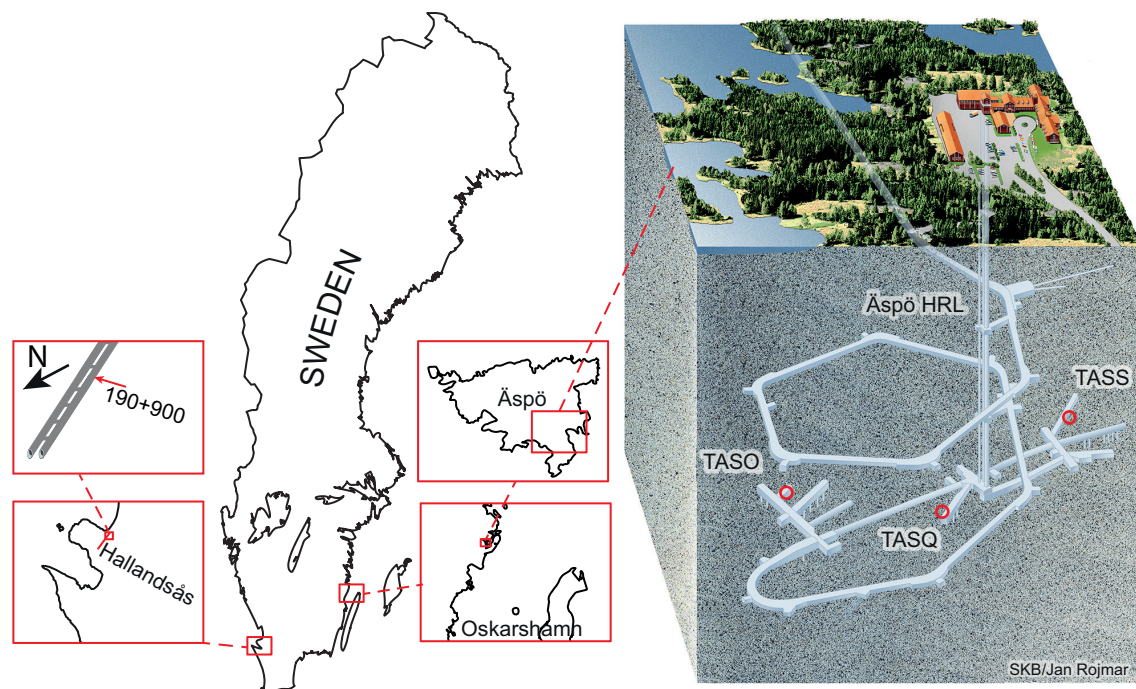


Figure 2: Left: Location of the Hallandsås tunnels and the test site at 190+900 m. Centre: The location of the island of Äspö in south-east and Hallandsås in south-west Sweden. Right: The layout of the Äspö HRL (before the 2012 expansion, used with permission from SKB) (Figure modified from Publication III)

2 LITERATURE REVIEW

In line with the overall aim, i.e. a fracture geometry description that results in increased accordance between hydromechanical and geomechanical fracture behaviour, this section provides an introduction to mechanical, hydraulic and hydromechanical descriptions of fractures. Since the focus in this work is on fracture geometry resulting from geological stress history, brief descriptions of tectonic and regional geological evolution and rock stresses are also provided.

2.1 Tectonic and regional geological evolution of the Fennoscandian Shield

In order to understand the behaviour of rock fractures, knowledge is needed about the origin, history and evolution of the fractures. There are a number of different geological processes that create fractures in rock. NRC (1996) identifies the following:

- Lithostatic changes, i.e. changes in the weight of the overburden
- Fluid pressure
- Tectonic forces originating from the movement of lithospheric plates
- Thermal processes; e.g. cooling of intrusive bodies or heating by radioactive waste
- Impacts from extraterrestrial objects
- Other activities, such as folding, volcanism and salt intrusions.

The main reason for stress build-up and fracturing is *plate tectonic activity*. Fractures formed due to *lithostatic changes* are mainly surficial since the effect is most significant near the surface. Fractures of these two geneses are the main focus in this description since they are important in describing the hydromechanical conditions in the Fennoscandian Shield in general and the two case study sites in this thesis in particular.

Unless stated otherwise, the following section is based on (Larsson and Tullborg 1993) and (Stephens et al. 2008). The Fennoscandian Shield¹ is one of the Earth's ancient continental nuclei and corresponds roughly to present-day Norway, Sweden, Finland and north-western parts of Russia (Figure 4). The majority of the Swedish bedrock belongs to three igneous provinces; The Svecofennian province, the Trans-Scandinavian igneous belt (TIB) and the South west Scandinavian Province. The rocks in the eastern part of Sweden were generally formed or reworked during the

¹ The term Fennoscandian Shield is preferred to Baltic Shield by the geological surveys of Sweden, Norway and Finland (Carl-Henric Wahlgren, SGU, personal communication 13-03-2013).

Svecofennian orogeny. The TIB is a suite of Granite-Syenitoid-Dioritoid-Gabbroid rocks formed 1.86 to 1.65 Ga.

The Sveconorwegian orogeny occurred about 1.1-0.9 Ga and resulted in complex, ductile deformation and metamorphism. Bulk crustal shortening occurred in an approximately WNW-ESE direction. The rocks of the Sveconorwegian orogeny are found in south-west Sweden and are sometimes referred to as the South-west gneiss province.

At approximately 600 Ma, the supercontinent Rodinia broke up and rifting of the crust occurred, which eventually resulted in the formation of the continent of Baltica. The Iapetus Ocean was opened as a consequence and Baltica moved northwards across the globe. Iapetus was closed again and Baltica collided with Avalonia and Laurentia during the Caledonian orogeny, where the Scandian mountain range was formed. During this orogeny, the Fennoscandian shield area was situated close to the equator and was shortened in a WNW-ESE direction (Stephens et al. 2008). A sedimentary cover was present east of the Caledonides, in central Sweden of up to 2.5 km thick, which accumulated after the Caledonian Orogeny and then have eroded away (Cederbom et al. 2000).



Figure 4: Generalised bedrock geology of the Fennoscandian Shield, modified from Wastenson and Fredén (2002).

During the Hercynian-Variscan orogeny, where Pangaea was assembled, the main tectonic activities had shifted southwards to the area of what is now central Europe. However, extensional deformations with igneous intrusions occurred in the Oslo rift and dextral transtensional deformation and mafic intrusions in the Tornquist Zone (Stephens et al. 2008).

During early Mesozoic, transtensional deformation occurred along the Tornquist zone, and later, during late Cretaceous-early Palaeogene, the Tornquist Zone was subject to dextral, transpressional deformation with maximum principal stress in a NNE-SSW direction (Stephens et al. 2008).

The North Atlantic started to open during early Palaeogene, and these movements are still ongoing. Due to the ridge push from the spreading North Atlantic, the major horizontal stress during Neogene to the present is roughly WNW-ESE or NW-SE (Stephens et al. 2008). Close to the Tornquist Zone, the major horizontal stress is roughly perpendicular to the zone, putting it under compression (Larsson and Tullborg 1993).

The large-scale fracturing pattern differs between the SW and SE part of Sweden, where the SE block pattern is more orthogonal and the SW part is more lensoid. The boundary between these patterns coincides approximately with the Protogine Zone. The Protogine Zone and, for example, the Tornquist Zone, which is where the Hallandsås ridge is situated, are examples of reactivated major shear zones (Larsson and Tullborg 1993).

Due to plate tectonic driven continental drift the Fennoscandian Shield has changed its position significantly since the original formation of its oldest rocks, see Figure 5 (Larsson and Tullborg 1993). The position on the globe covers a 60°N position, similar to the present, down to 60°S and back north again. Significant rotation has also occurred (Larsson and Tullborg 1993). The overall crustal plate configuration and changes in the configuration are even more dramatic but are not included in Figure 5. The period of 100 - 200 Ma resulted in deep weathering, when the Fennoscandian shield was situated further south, and during this warm Triassic-cretaceous period the fracture zones of the Tornquist Zone were exposed to deep weathering.

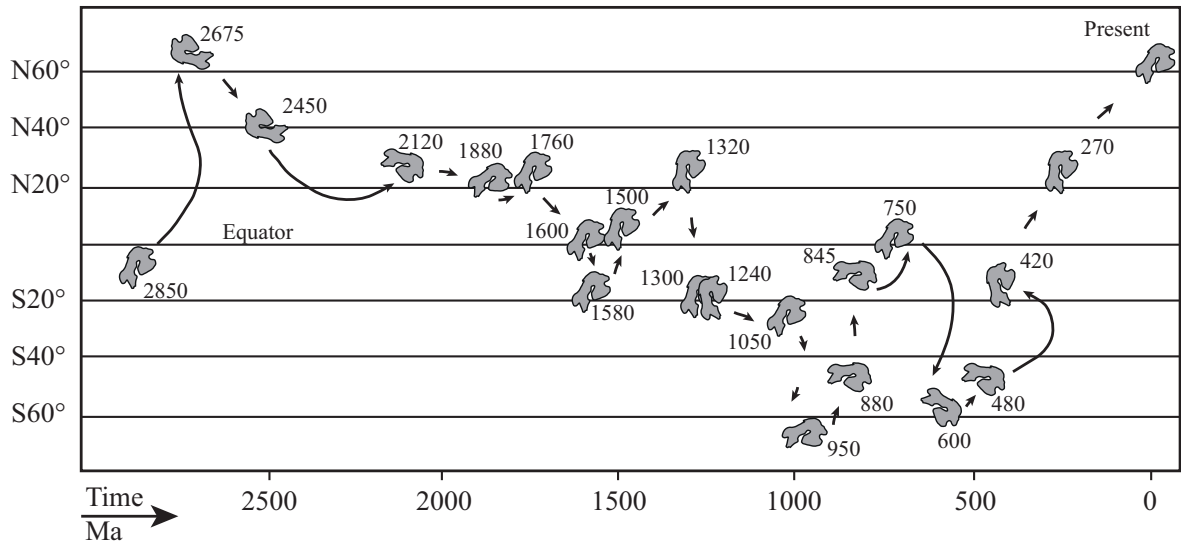


Figure 5: A diagram of the latitudes and rotation of Baltica from 2850 Ma ago up to the present, adapted from Larsson and Tullborg (1993). During the last movement northwards, the bedrock of the Fennoscandian shield was subject to deep weathering, which can still be seen in the fracture zones at Hallandsås.

2.1.1 Tectonic evolution of the Äspö area

Äspö lies in the SE part of Sweden (Figure 2). The fractures of the Äspö rocks were generated, later filled with mineral precipitates and eventually reactivated during different tectonic events, Figure 6. The initial formation of the rock is associated with the Svecofennian Orogeny, about 1.8 Ga ago, as well as intrusions of the Götömar granite, 1.4 Ga. In Figure 6, the upper part is a schematic description of the large scale tectonic activities that the area has been through. The boxes in the lower centre exemplify the events and appearance on a local scale. At the bottom historical stress regimes are outlined, see further about the present stress regime in section 2.2.1.

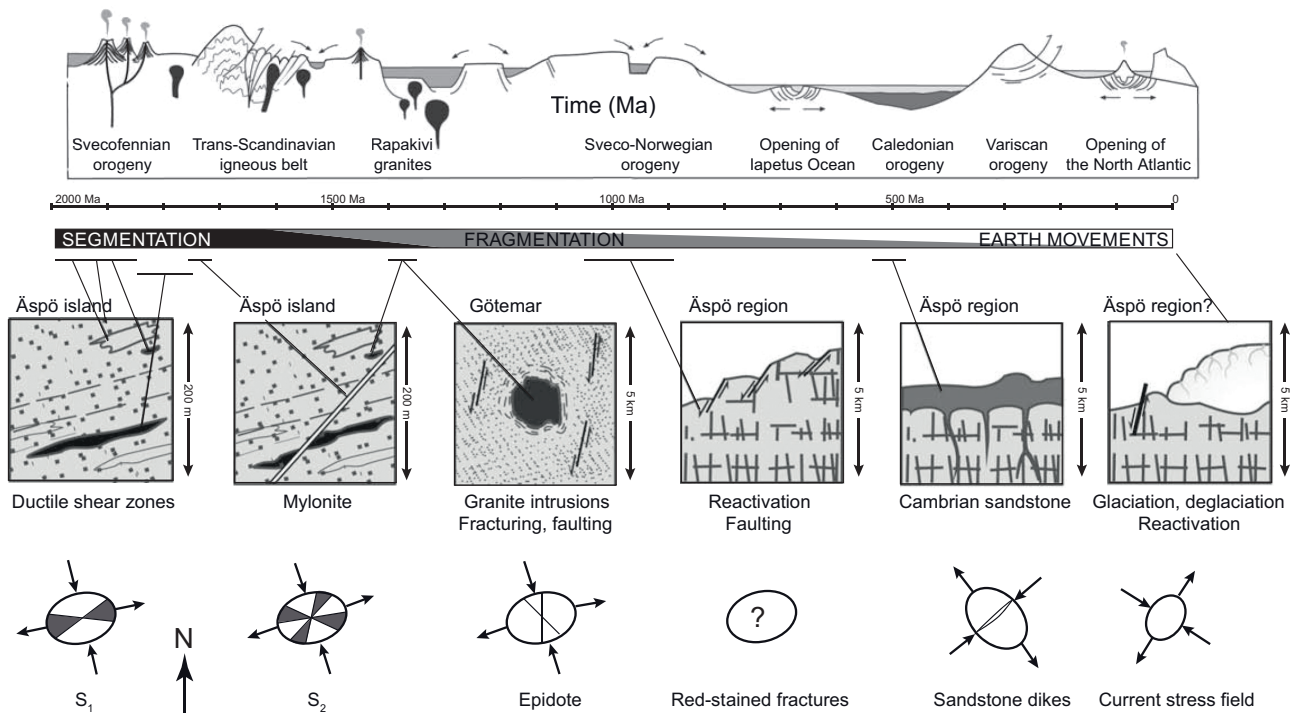


Figure 6: A schematic illustration of the geological evolution of the Äspö area, (Gustafson 2012), after Munier (1993).

2.1.2 Tectonic evolution of the Hallandsås area

The rocks of Hallandsås were originally formed about 1.7 Ga ago and were subject to regional metamorphism linked to the Sveconorwegian orogeny 1.1-0.9 Ga ago. The Tornquist Zone, where Hallandsås is situated, has been reactivated numerous times with a series of brittle deformations and faulting during the last 300 Ma, see Figure 7. The largest movements occurred about 70 Ma, and since then several horsts have been present in the area, one of which is Hallandsås (Sturk et al. 2011). The bedrock contains a dense pattern of faults that has been subject to extension and compression as well as deep weathering. Dolerite/amphibolite dyke intrusions contributes to the complex, present-day situation (Kvartsberg et al. (submitted)).

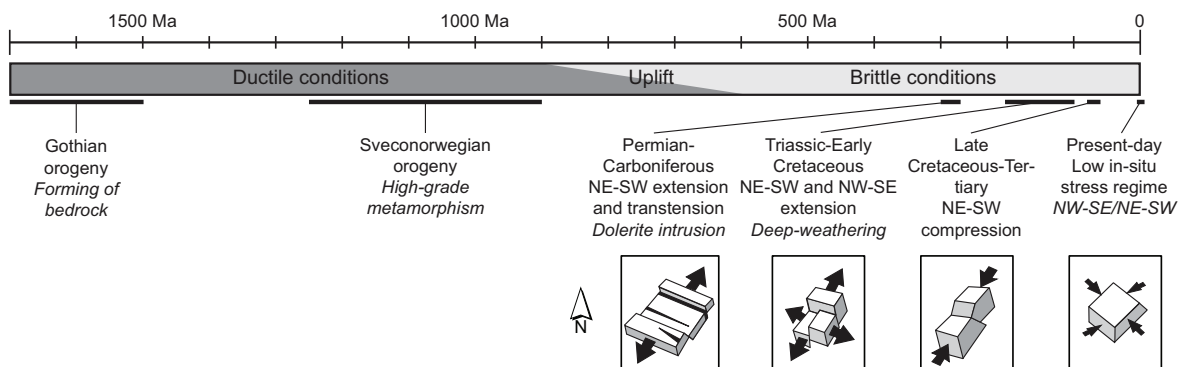


Figure 7: A schematic illustration of the geological evolution of Hallandsås, from (Kvartsberg et al. (submitted)).

2.2 Stress conditions

Any given rock volume is subject to rock stresses that mainly originate from the weight of overlying rock, plate tectonic movements, glaciostatic recovery and fluid pressure. The respective importance and orientation of these contributors may vary between different sites.

2.2.1 In situ rock stresses

The state of in situ stress across the Fennoscandian shield has been measured for various engineering, mining and research purposes over the last few decades. Some 500 entries of rock stresses were reported in the Fennoscandian Rock Stress Data Base, FRSDDB (Stephansson et al. 1987), a regional predecessor to the World Stress Map. Stephansson et al. (1991) conducted regression analysis of hydraulic fracturing data from the FRSDDB, which together with a measure of vertical stress as the weight of the overburden ($\rho \cdot g$) (1) provides the following rules of thumb for the major horizontal rock stress σ_H (2), the minor horizontal stress σ_h (3) and the vertical rock stress σ_v at depth z , and.

$$\sigma_v = \rho \cdot g \cdot z \quad (1)$$

$$\sigma_H = 2.8MPa + 0.04z \quad (2)$$

$$\sigma_h = 2.2MPa + 0.024z \quad (3)$$

In the Fennoscandian shield, the horizontal stresses are generally larger than the vertical stress, Stephansson et al. (1991) suggest minor effects from uplift after the latest glaciation and larger effects from rock creep due to the ice loading and ridge push from the mid-Atlantic ridge.

The orientation of the stresses scatter to a large extent although a trend of σ_I alignment perpendicular to the mid-Atlantic ridge can be seen at depths greater than 300 m. The stresses close to fracture zones are affected by the zones due to their limited ability to transfer the stresses. If a zone is unable to transfer shear stresses, the stress field will bend to be perpendicular to the zone. Hakami et al. (2002) conducted a review of the stress state in Sweden and stated that the effect of the latest glaciation was significant to the stress field but that it is now back to a stress field dominated by plate tectonics.

With a large scatter in the general trends and disturbances near zones, site-specific data will be needed for most cases. This thesis deals with case studies from

Hallandsås and Äspö HRL and the stress situation at these particular sites is described further below.

The rock stresses at the Äspö HRL are divided into two domains by the zone NE-2 (Ask 2004). Close to this zone, the major principal stress, σ_1 , strikes 128°N and dips 0-19°, while σ_2 , and σ_3 are roughly equal in magnitude with complexly varying orientations.

Included in the cases presented in this thesis are samples from slabs that were sawn out of the TASS and TASQ Tunnels (Paper III) as well as in situ measurements in the TASO Tunnel (Paper II). TASO is situated east of the NE2 zone, TASS west of it, while TASQ is close to NE2 on the western side (see Figure 2 for the tunnel positions in the HRL). Stress measurements from the three tunnels can be seen in Table 1.

Table 1: The rock stress situation at the three relevant tunnels on the 420 - 450 m level of Äspö HRL.

Site	TASQ (Staub et al. 2004)		TASS (Hakala et al. 2012)		TASK/Demo, near TASO (Janson and Stigsson 2002)	
	Magnitude (MPa)	Trend°	Magnitude (MPa)	Trend°	Magnitude (MPa)	Trend°
Depth	- 450 m		- 450 m		- 420 m	
°RT90						
σ_H	30	310	23-24	136-139	16-26	140-155
σ_h	10	208	12-13	-	9-14	-
σ_v	15	-	10-11	-	10.5-18.1	-

Hallandsås is a gneiss horst within the line of faults of the Tornqvist Zone. There are dolerite dykes, amphibolites, heavy fracturing and faulting, deep weathering and large amounts of groundwater, making the geology complex (Sturk et al. 2011). Since Hallandsås is a fractured and faulted horst, the stresses are low and irregular and the horizontal stresses lower than the general trends for Fennoscandia presented above. Sturk et al. (2011) state that the vertical stress, σ_v is equal to the weight of the overburden, σ_H is equal to that or lower and perpendicular to the tunnel (i.e. roughly parallel to the horst length axis) and σ_h is significantly lower. An earlier rule of thumb that served as a basis for Paper I was that $\sigma_v = \sigma_h$, $\sigma_H = 2\sigma_v$ (Runslätt and Thörn 2010).

2.2.2 Stresses induced due to excavation

Up to now, the primary in situ stresses have been the topic but when a tunnel is excavated, the stress field needs to redistribute around the tunnel, rendering induced stresses. The general feature is that a disturbance in the stress field occurs around the opening and decreases the greater the distance from the opening. Kirsch (1898) (see e.g. Lindblom (2010)) presented a solution to the induced stresses around a circular opening in a homogenous plate, see (4), (5), (6) and Figure 8.

$$\sigma_r = \frac{1}{2} \sigma_z \left((1+k) \left(1 - \frac{a^2}{r^2} \right) + (1-k) \left(1 - 4 \frac{a^2}{r^2} + 3 \frac{a^4}{r^4} \right) \cdot \cos 2\theta \right) \quad (4)$$

$$\sigma_\theta = \frac{1}{2} \sigma_z \left((1+k) \left(1 + \frac{a^2}{r^2} \right) - (1-k) \left(1 + 3 \frac{a^4}{r^4} \right) \cdot \cos 2\theta \right) \quad (5)$$

$$\tau_{r\theta} = \frac{1}{2} \sigma_z \left(-(1-k) \left(1 + \frac{a^2}{r^2} - 3 \frac{a^4}{r^4} \right) \cdot \sin 2\theta \right) \quad (6)$$

Where σ_r is the radial stress, σ_θ is the tangential stress, $\tau_{r\theta}$ is the shear stress, k is the ratio σ_x/σ_z , a is the tunnel radius, r is the radius to the calculated point and θ is the angle between the vertical centreline and the calculated point, see Figure 8.

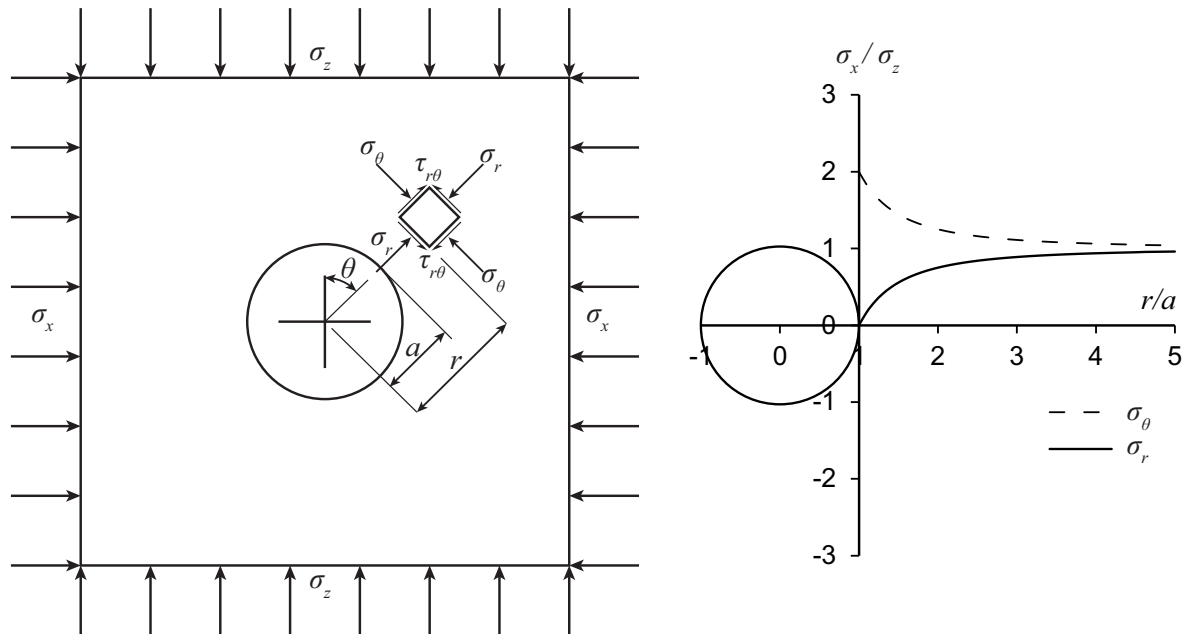


Figure 8: Left: The stress field in a plate with a circular opening, according to (Kirsch 1898) (After (Lindblom 2010)). Right: A plot of the radial stress, σ_r , and the tangential stress, σ_θ , and their variation with distance from the tunnel wall.

The Kirsch equations applied to a stress field, as shown in Figure 8 result in a concentration of tangential stress near the opening. Correspondingly, the radial stress will experience relief. For a tunnel in the common in situ case with horizontal stresses larger than the vertical stresses, the walls will experience stress relief. Stress concentrations occur in the roof and floor.

Applying the Kirsch equations to the rock mass close to a tunnel implies certain simplifications. A tunnel in a rock mass, generally horseshoe-shaped, is heterogeneous in 3D, while the Kirsch equations deal with a homogenous material in a 2D case. This means that the effect of the stress field adapting to the orientation of fractures cannot be captured.

Stress estimations for the in situ conditions of the slabs from TASS were made in Ericsson et al. (2009). The distinct element code Examine 2D (Rocscience 2010) was used. Examine 2D can deal with complex excavation geometries in 2D sections without fractures in the rock mass. An estimation of the normal and shear stresses acting on the specific sampled fractures from the TASS slabs was made for Publication III. The stress components from the Examine 2D output data were transformed to the strikes and dips of the fractures.

2.2.3 Groundwater pressure

An undisturbed and unmoving groundwater pressure head is hydrostatical, i.e. equal to the depth to the groundwater surface. The groundwater pressure at a given depth is then achieved by multiplying the depth by the density of water and acceleration due to gravity. However, this is a significant simplification and just as for stresses, site-specific data is needed for most applications.

Inside a tunnel with air of atmospheric pressure, the groundwater pressure is equal to zero and the gradient of increasing pressure from the tunnel wall out to undisturbed conditions depends on the fracture system and the sealing of the system.

At Äspö HRL, groundwater pressure is monitored in many boreholes and pressures of 3.5-3.8 MPa are fairly common at the 450 m level, indicating that the pressures are not fully hydrostatical. In boreholes closer to the tunnel system, pressures ranging from 0 to 3.5 MPa are common (Wass and Nyberg 2009). In the specific boreholes tested at Hallandsås, groundwater pressures of up to 0.5 MPa were measured (Runslätt and Thörn 2010). The rock cover at the site was about 75 m.

2.2.4 Effective stresses

The principle of effective stresses was introduced by Terzaghi (1936) for saturated soil (Olsson 1997). The groundwater pressure, u , will help carry and distribute part of the load from the overburden, σ , giving an effective stress σ' as (7). This is valid for an incompressible, porous solid filled with an incompressible inviscid liquid (Bluhm and Boer 1996). In the case of fractured rock with low matrix porosity, a correction factor, α (0-1), may be introduced (8). Kranz et al. (1979) identified the need for a correction for (7) but did not express it in terms of α . Further, (Kranz et al. 1979) argue that the correction is dependent on the stress history and surface roughness of the fracture in question and that “there is no *simple* effective stress law for the permeability of jointed rock”. Olsson (1997) concludes that for a low stress rock mass α should be equal to unity, since the area of contact inside the fracture is small and the pore pressure is able to attack most of the fracture surface area, whereas for higher stresses α may be 0.9.

$$\sigma' = \sigma - u \quad (7)$$

$$\sigma' = \sigma - \alpha \cdot u \quad (8)$$

2.2.5 Stress measurements

The level of rock stress can be measured by disturbing the in situ conditions and monitoring the results or by observing rock behaviour without significant influence from the measurement method. This description focuses on the former and is mainly based on Ljunggren et al. (2003).

Three types of measurement methods are included in the group 'hydraulic methods and surface relief methods', which investigate rock volumes generally in the order of one to tens of cubic metres, as well as 'borehole relief methods', which investigate significantly smaller volumes. Surface relief methods include measurement between pins or gauges on a rock surface before and after the rock volume is stress-relieved by drilling or cutting it free from the stress field (Ljunggren et al. 2003).

Two hydraulic methods are common, hydraulic fracturing, HF, and hydraulic tests of pre-existing fractures, HTPF. Both methods are usually performed in vertical boreholes from the surface. In HF, roughly one metre of a borehole is pressurised between straddle packers until the rock breaks and an increased flow or pressure drop is recorded. The rock breaks where the least resistance is offered – perpendicular to the minor horizontal stress – and the orientation can be measured using an impression packer. The magnitude of the minor horizontal stress is determined by lowering and raising the pressure and identifying when the fracture

opens and closes from the flow data. HTPF works in a similar way but with pre-existing fractures. At least six different fractures are needed to calculate the stress orientations and magnitudes (Ljunggren et al. 2003).

Borehole relief methods generally refer to overcoring methods where a probe is installed in a core borehole. The deformation of the rock adjacent to the probe is measured while a larger borehole is drilled around the probe, relieving the stress. A number of sensors are needed in each probe as well as measurement of at least three non-parallel boreholes to calculate the stress field (Ljunggren et al. 2003).

2.3 Geological and geometrical description of fractures

This section describes fractures as geometrical entities that make up a more or less systematic network in the rock mass, as well as the appearance of individual fractures.

Fractures are grouped in sets defined by their similar orientations. Usually, there are a few sets present in any given rock volume. At Äspö HRL, there are six fracture sets that make up 92% of 11,000 fractures mapped during the construction of the main tunnels up to 2001 (Talbot and Sirat 2001). The fractures in a set may have the same genesis and similar properties.

Fracture intensity refers to the number of fractures per investigated rock quantity. Dershowitz and Herda (1992) list the available intensity measurements, depending on the number of dimensions of the fracture measurement and the investigated region. Hernqvist (2009) comments that measurements using the unit m^{-1} are preferable as they are scale-independent and practical for field use. The measurements are the number of fractures along a scanline, metres of fracture trace on a surface and fracture surface in a volume. The first two could be expected to be more easily obtainable.

With fracture sets and fracture intensities, the fracture system will show a certain degree of connectivity, which is a measure of the connections between different fractures. The connectivity is interesting from a hydrogeological point of view and the water-conducting ability of the individual fractures will determine if and to what extent water can flow from one part of the system to another.

When it comes to a description of individual fractures, the fracture void geometry reveals a number of properties and the presence of mineral precipitates or gouge products in the void could affect the properties in various ways. Hakami (1995) mentions eight such properties: aperture, i.e. the distance between the surfaces; the

contact area between the surfaces; the roughness and matedness of the surfaces, i.e. how coarse the surfaces are and how well they fit together; the spatial correlation; presence of channelling, i.e. continuous, wider paths that may transmit water; tortuosity, i.e. un-straightness of flow paths; the stiffness across the surfaces, i.e. the measure of the stress needed to bring the surfaces one length-unit closer to each other.

2.3.1 Deformation zones

The term *deformation zone* is defined in the SKB site descriptive work as a sub-planar structure with a small thickness in relation to its in-plane extent, where deformations have been (or are) concentrated (Munier et al. 2003). As for fractures that are sub-divided into joints and faults depending on their style of development, further items of information on the deformation zone could facilitate a more precise designation. The commonly used term *fracture zone* would refer to a brittle deformation zone or the brittle part of a *composite deformation zone*. A *composite deformation zone* shows evidence of both brittle and ductile deformation, commonly as a brittle reactivation of a *ductile deformation zone* (Munier et al. 2003).

A brittle zone, being a concentration of fractures, is likely to be more transmissive than the host rock. If the zone has undergone shear movements, it is designated a fault. An extensive review of recent research on faults is carried out in Faulkner et al. (2010). They present a simple, conceptual model of the structure of a fault, the *protolith-damage, zone-fault core* model. A concentration of fractures is observed in the damage zone and, if present, the core is one or more segments of crushed rock, gouge and cataclasites. The damage zone acts as a hydraulic conduit, while the core may act as a barrier.

2.3.2 Aperture, contact geometry and roughness

There is no universal agreement on terminology related to apertures. Jing and Stephansson (2007) state that *geometric aperture* is the nominally normal distance between the two rough but nominally planar surfaces of a fracture. Assuming that the mean planes of the two rough surfaces are parallel, the *mechanical aperture* is the distance between them. The *hydraulic aperture* is then related to the void that actually conducts water. Conceptually, the magnitude of these three apertures is in the order mentioned, with hydraulic aperture being the smallest (Jing and Stephansson 2007), see Figure 9.

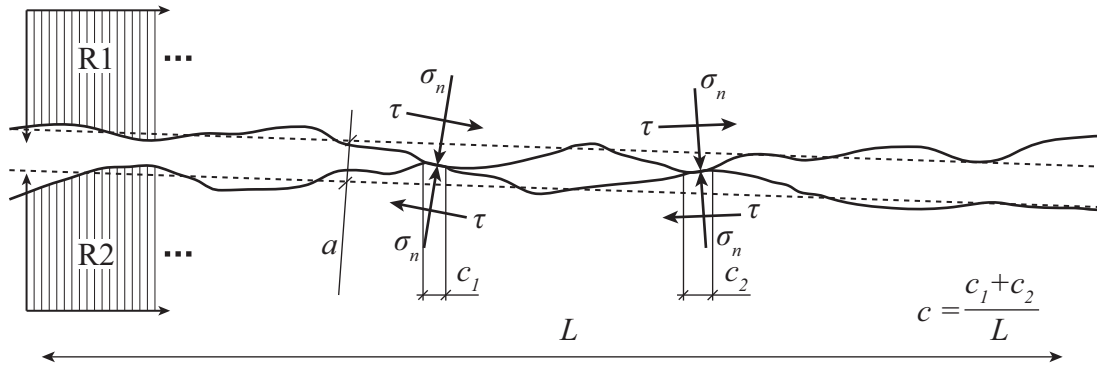


Figure 9: The roughness of the two fracture surfaces, R1 and R2, aperture of the fracture, a , and contact area, c , (in this 2D representation what can be seen is contact length). Mechanical loads are transferred through the contacts (σ_n, τ).

Roughness is a measure of the surface height distribution, or unevenness of fracture surfaces (Figure 9). It is linked to aperture, which is defined from the combined roughness of the two sides of a fracture (Hakami 1995). Barton (1973) defined an empirical roughness parameter, JRC, (9) that has been widely used in engineering practice (Fardin et al. 2001) and was initially developed for studying the shear strength of fractures (Legrain and Tshibangu 2006).

$$JRC = \frac{\tan^{-1}\left(\frac{\tau}{\sigma_n}\right) - \phi_b}{\log\left(\frac{\sigma_c}{\sigma_n}\right)} \quad (9)$$

where τ is the peak shear strength, σ_n is the normal stress, ϕ_b is the friction angle and σ_c is the rock compressive strength, which is replaced by JCS (joint compressive strength) for weathered joints. The JRC coefficient ranges from 20 (rough) to 0 (smooth), and the parameters for (9) can be determined either by push, pull or tilt tests (Fardin et al. 2001). JRC can also be assessed by comparing the fracture profile with the type profiles defined by Barton and Choubey (1977), see Figure 10.

Efforts have been made to correlate the JRC value with statistical parameters of fracture geometry. Some have a strong correlation with JRC although JRC varies both in scale and between different fractures (Fardin et al. 2001). Tatone and Grasselli (2009) developed a 3D method for measuring and describing the roughness of a surface. Tatone and Grasselli (2010) also developed a corresponding

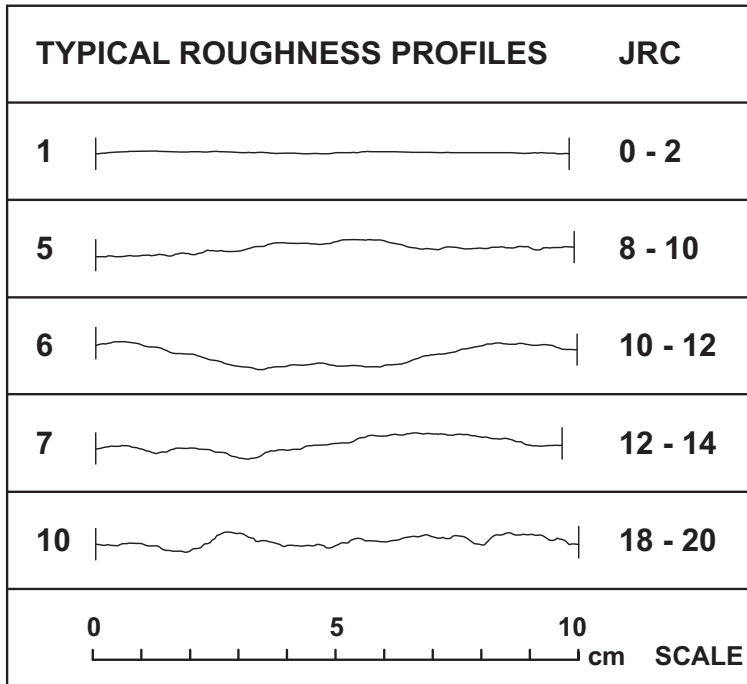


Figure 10: Selection of type profiles of fracture roughness and their corresponding JRC, presented by (Barton and Choubey 1977).

2D method and provided a correlation to JRC. The correlation was based on analysis of the type curves in Figure 10, somewhat rotated, and a power-law relationship was used. (Legrain and Tshibangu 2006) provided correlation between JRC and fractal dimension.

Fractals are a class of mathematical functions that have an inherent scale independency and are therefore appropriate for describing different geological phenomena, which are usually scale independent. There are two forms of fractals, self-similar and self-affine (Brown 1995a). Self-affine fractals are suitable for describing natural and artificial rock fractures (Power and Durham 1997; Fardin et al. 2001). Consequently, further discussion of fractals focuses on self-affine fractals.

All natural rock surfaces can be described, to a first approximation, using a power spectral density function of the form (10).

$$G(k) = Ck^{-\alpha} \tag{10}$$

Where $k = 2\pi / \lambda$ is the wave number and λ is the wavelength along the profile. C is a proportionality constant that varies between surfaces and the power α usually varies between $2 < \alpha < 3$ (Brown 1995a).

The dimension of a fractal, D , describes its scaling properties and is a measure of its roughness (Brown 1995a). D alone is not sufficient to describe surface roughness

and it needs to be supplemented by amplitude or *rms* roughness (Olsson 1998; Brown and Scholz 1985; Brown 1995b; Fardin et al. 2001)

The roughness of each side, as well as the aperture, can also be expressed as an average value with a lognormal standard deviation. However, this representation is scale dependent and cannot be applied to other sample sizes or scan resolutions.

The two surfaces of a fracture are in contact at certain points where compressive and shear stresses are transferred. However, the definition of contact is difficult, since there is no sharp border between contact and non-contact, even on a microscopic scale. Hakami (1995) used a threshold aperture of 1 μm to define contact points for small-scale applications. The contact area for a fracture is expressed in terms of percentage contact and varies widely from one fracture to another and various stress conditions.

Measurement of contact geometry and aperture has been performed in different ways. Metal casts with Wood's metal is one such method, where the convenient melting point of the alloy makes it possible to use with regular lab equipment. Pyrak-Nolte et al. (1987) used this method. Other methods are moulding transparent fracture replicas and using dyed water (Hakami 1988), silicone rubber (Gentier et al. 1989) or laser scanning of the surfaces (Lanaro 2001) to characterise the fracture void geometry.

Nemoto et al. (2009) used pressure-sensitive plastic film between the fracture surfaces during compression tests and then scanned the film to obtain aperture maps at different levels of stress. The film is readily available and contains a layer of microcapsules containing dye, which are ruptured at a certain level of stress. The dye changes in contact with the adjacent layer of the film, tinting it to different intensities of red depending on the stress (Fujifilm 2010) (Nemoto et al. 2009) In the case of pressure-sensitive film, the threshold for contact must also be defined. (Nemoto et al. 2009) found it appropriate to set the threshold at a local minimum between the two peaks, which was evident from their colour intensity histograms.

2.3.3 Fracture infillings and alterations

During a tectonic event, one or more of the fracture sets that is present in the rock mass are generally altered. The alterations could be shearing under different degrees of confining pressure, which give rise to different amounts of gouge products and degrees of flattening of the asperities. Other alterations may be weathering of the rock close to a fracture where aggressive and/or hot groundwater has circulated. Yet another type of alteration is the precipitation of minerals that

were in solution in the groundwater. Minerals may precipitate to such an extent that the fracture can be regarded as completely sealed. Different fillings have different mechanical properties and thus affect the fracture in different ways. Soft minerals may reduce the friction and shear resistance of a fracture while hard minerals may have the opposite effect. The presence of any solid material between the fracture surfaces affects the fluid flow in the fracture.

For Äspö HRL, Drake and Tullborg (2009) outline six generations of fracture minerals, see Table 2. These mineral generations were formed at different phases of tectonic stress and temperature throughout history, in both new and reactivated older fracture sets, see Figure 6. The first generation of fracture fillings was dominated by quartz and epidote and occurred mainly in fractures striking N-NNW as well as in sub-horizontal directions. Chlorite was precipitated over a long period of time, over several generations. Chlorite appears in the same fracture sets as the older mineral fillings, as well as a steep WNW-NW set. Calcite is the dominating mineral for the latest fracture mineralisations and appears mainly in older, reactivated fractures. The WNW set is common for fractures bearing calcite and other minerals as well as fractures with calcite only. The WNW set was therefore probably the latest to reactivate (Munier 1995).

Hallandsås has been subjected to heavy faulting and clay weathering. Hence, apart from crushed fault core there is smectite-weathered amphibolites and in deep fractures kaolin weathering is common (SOU 1998).

Table 2: Fracture mineral generations for the Laxemar area, adjacent to Äspö, from Drake and Tullborg (2009).

Gen	Description	Dominating minerals	Approx. age (Ma)
1	Mylonite	Epidote, quartz, muscovite	1400
2	Cataclasite	Epidote, chlorite, adularia, quartz, hematite	-
3	Coarse-grained, sealed fractures	Quartz, calcite, pyrite, chlorite, epidote, prehnite, laumontite, adularia, muscovite	1420
4	Thin, sealed fractures	Calcite, adularia, laumontite, quartz, chlorite, illite, hematite	990
5a	Sealed or open fractures	Calcite, pyrite, <i>Mixed layer clay</i> , chlorite, fluorite	400-450
5b/6	Open fractures	5b: same as 5a. 6: Calcite, clay minerals, tyrite, goethite	- -

2.4 Mechanical description of fractures

This section introduces basic concepts of fracturing in rock and some applicable models to describe the mechanical response in terms of fracture stiffness.

2.4.1 Mohr Coulomb failure

The Mohr-Coulomb failure criterion is based on a set of linear equations in the principal stress space that governs the failure of an isotropic material (Labuz and Zang 2012). The effect of the intermediate principal stress, σ_2 , is generally ignored but it could be included if the 3D realisation of the failure criterion is used together with true triaxial experimental data (Labuz and Zang 2012). The 2D realisation, i.e. with no regard to, σ_2 , can be adopted graphically in a Mohr diagram (Figure 11). When a circle between the major and minor principal stresses in the Mohr diagram reaches the failure envelope defined by the cohesion, c , and friction angle, ϕ , a shear failure occurs, usually at the angle $\alpha_f = 45^\circ + \phi/2$ (Gustafson 2012). Tensional failure can be handled by curving the envelope on the negative side of the σ -axis so that it reaches the σ -axis at $\sigma = -T$, i.e. the tensional strength.

In the case of reactivation of a pre-existing shear fracture, Hakami et al. (2002) states that the failure envelope is moved downward in the Mohr diagram, corresponding to a lack of cohesion, $c = 0$ (Figure 11). Furthermore, they argue that the friction angle is changed, often to a lower value than before the initial failure. In the Figure 11 example, reactivation of fractures with angles between β' and β'' to the major principal stress, σ_1 , is possible.

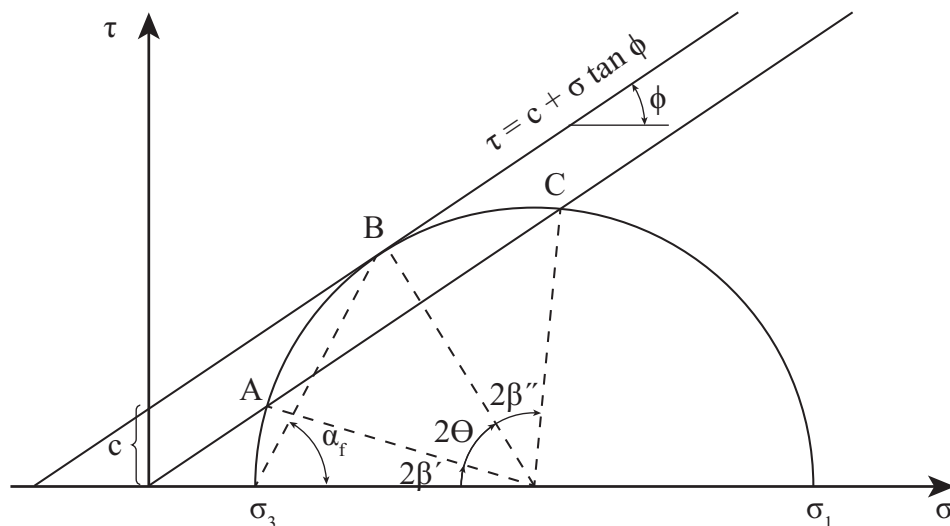


Figure 11: A linear Mohr-Coulomb failure envelope in a Mohr diagram and adjusted (lower) envelope for shear reactivation where shear failure may occur between the angles β' and β'' (Inspired from Hakami et al. 2002; Gustafson 2012; Labuz and Zang 2012).

2.4.2 Ideal fracture patterns

Ideal Mohr-Coulomb fracturing on a larger scale in an intact isotropic medium produce a systematic rhombic fracture pattern, as seen in Figure 12. A supplementary set of tensional fractures may form parallel to the major stress direction.

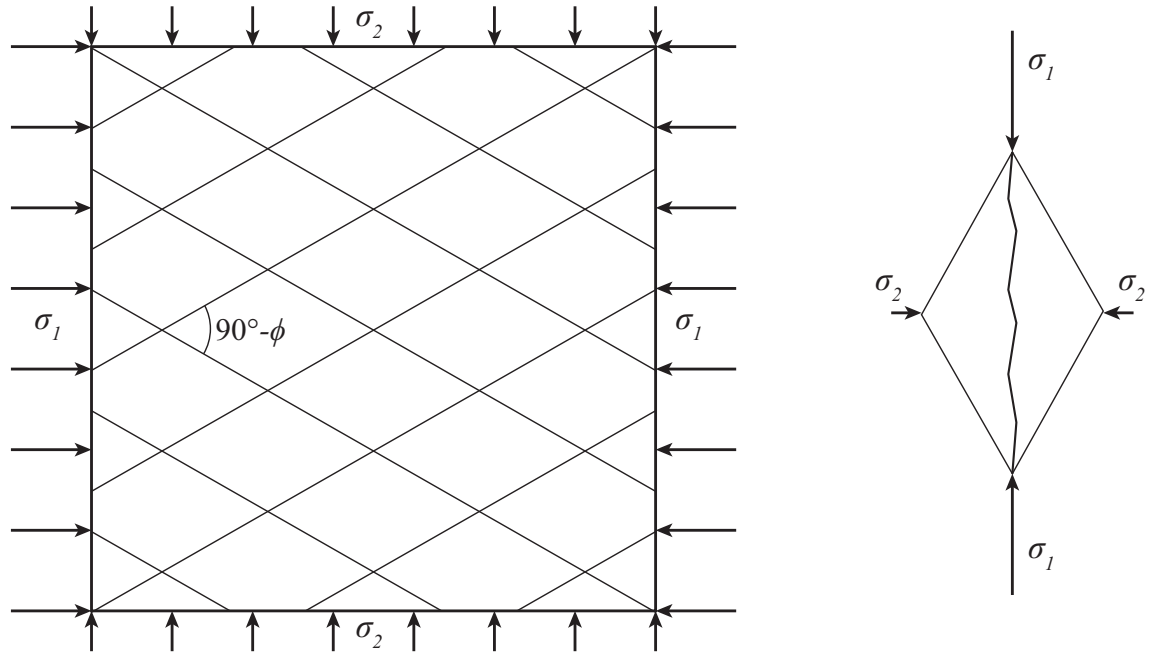


Figure 12: Left: Rhombic Coulomb fracturing of an intact rock block with a friction angle ϕ , due to the stresses $\sigma_1 > \sigma_2$. Right: The formation of a tension fracture in a stressed rhombic block. According to Gustafson (2012).

The formation of younger fractures is influenced by the presence of older fractures. If the older fractures cannot sustain any shear stresses, the younger fractures will curve and terminate at a 90° angle to the older fracture (Hakami et al. 2002). For higher shear strength of the older fractures, this effect will be less prominent up to the stage where the shear strength of the old fracture is similar to that of the intact rock. In that case, the younger fracture can cross the older one without any change in orientation (Hakami et al. 2002). The effect can be seen at a larger scale also, Rawnsley et al. (1992) identified joint sets that bend towards a regional-scale fault.

2.4.3 Fracture stiffness

The behaviour of fractures prior to an ultimate failure was studied by Goodman (1970) (see e.g. Rutqvist and Stephansson 2003) He expressed normal and shear deformation of fractures as a function of stiffness and applied stress (15). Δu_n is called normal closure, and is defined as positive when the aperture decreases.

$$\begin{aligned}\Delta u_n &= k_n \Delta \sigma_n' \\ \Delta u_s &= k_s \Delta \sigma_s\end{aligned}\quad (11)$$

With the designations used here, normal stiffness can be expressed as the effective stress change divided by the change in aperture for the same stress change (16). The same applies to shear stiffness and normal stiffness from hydraulic aperture change.

$$k_n^a = \frac{\Delta \sigma'}{\Delta a}\quad (12)$$

Goodman (1974, 1976) (see e.g. Rutqvist and Stephansson 2003) showed through experiments that the deformation of an intact sample was smaller than for a sample with a mated fracture, which was in turn smaller than for a unmated fracture. The deformation was highly nonlinear and he proposed the hyperbolic closure relationship (13)

$$\Delta u_n = \frac{\sigma_{ni}'}{k_{ni}} \left(1 - \frac{\sigma_{ni}'}{\sigma_n'} \right)\quad (13)$$

Where σ_{ni}' is a low initial stress and k_{ni} the initial normal stiffness.

Based on extensive laboratory testing, Bandis et al. (1983) suggested an empirical constitutive model that has proved important for practical applications and have been the most commonly used (Rutqvist and Stephansson 2003) The description is a hyperbolic function, (14)

$$\delta = \frac{\sigma_n'}{k_{n0} + \sigma_n' / \delta_m}\quad (14)$$

Where δ is the current normal closure, k_{n0} is the normal stiffness at the zero stress intercept and δ_m the maximum normal closure. The latter two can be estimated from JRC_0 and JCS_0 (Barton et al. 1985).

The Evans model (Evans et al. 1992) (see e.g. Rutqvist and Stephansson 2003) uses a logarithmic relationship that applies to third or later load cycles. It matches in particular the deformation behaviour of unmated fractures but fails to reproduce a residual aperture and can therefore only be applied to stresses up to about 10 MPa. (15).

$$-\Delta u_n = \frac{1}{dk_n/d\sigma_n'} \ln \left(\frac{\sigma_n'}{\sigma_{n0}'} \right)\quad (15)$$

where $dk_n/d\sigma_n'$ is designated *stiffness characteristic* and can be evaluated from a stress-deformation plot. The normal stiffness, k_n , can be expressed as (16).

$$k_n = (dk_n/d\sigma_n')\sigma_n' \quad (16)$$

Zangerl et al. (2008) compiled data for 115 laboratory and in situ normal closure experiments. Most of the data originated from granitic rock and the resulting stiffness characteristic values varied widely. However, the semi-logarithmic closure law proved accurate.

2.5 Hydraulic description of fractures

This section provides a background to the flow of groundwater in fractures and some experimental methods for quantifying the flow properties.

2.5.1 Darcy's Law

Darcy (1856) described the flow due to a gradient in a porous medium, (17) and this is nowadays referred to as Darcy's law, see e.g. Fetter (2001).

$$Q = -K \cdot A \frac{dh}{dl} \quad (17)$$

where Q is the flow, K is the hydraulic conductivity, A is the cross-section area of the flow medium, and dh/dl is the gradient of the hydraulic head.

Since its introduction in 1856, Darcy's law has been applied to 2D and 3D calculations as well as the flow in rock fractures to which the porosity of crystalline rock mass is highly concentrated. Darcy's law applies to laminar flow of the fluid, which can be checked by calculating the Reynolds number (18)

$$R_e = \frac{\rho \cdot v \cdot D_f}{\mu} \quad (18)$$

where ρ is the density of water, v , is the velocity of flow, D_f is the hydraulic diameter, defined as four times the fracture cross-section area divided by the circumference of the same area, and μ is the viscosity of water.

The transition between laminar and turbulent flow occurs at a different Reynolds number for smooth fractures (parallel plate) and rough fractures. Zimmerman and Bodvarsson (1996) provided criteria for these transitions, adapted graphically in Gustafson (2012), see Figure 13.

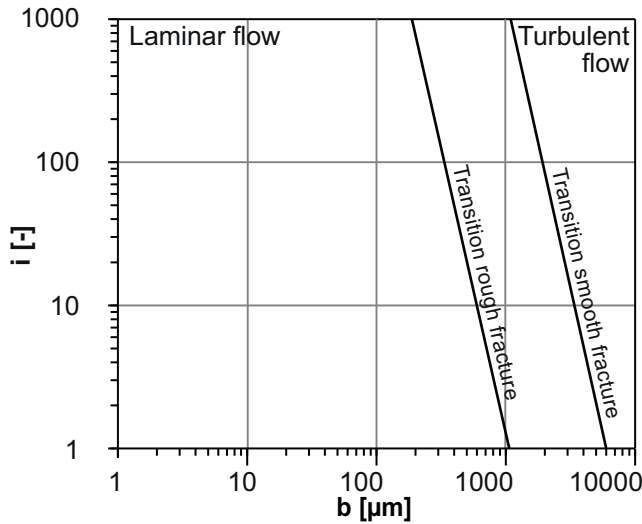


Figure 13: Hydraulic gradient, i , (or dh/dl) and hydraulic aperture, b , in relation to the transition from laminar to turbulent flow.

2.5.2 Conductivity, transmissivity and storage coefficient

Darcy's Law has three components: the gradient of the hydraulic head, the cross-section area of the flow medium and a proportionality parameter – the hydraulic conductivity K [m/s]. The conductivity concept is well suited to a description of flow in granular or porous material. For fractured crystalline rock where the water flow is highly concentrated to the fractures, transmissivity is a better measure (Gustafson 2012). Transmissivity is expressed as the conductivity, K , multiplied by the thickness of the aquifer or fracture, b , which gives T [m²/s].

When an aquifer is subject to hydraulic head changes, it will absorb or expel water. The amount of water stored or expelled is a material parameter called storativity or storage coefficient, S [-]. Storativity is the volume of water storage per square metre of aquifer and metre of head change and is thus dimensionless (Fetter 2001). Storativity can be estimated as (19) (Doe and Geier 1990).

$$S = \rho_f \cdot g \left(\frac{1}{k_n} + e_v \cdot C_f \right) \quad (19)$$

where ρ_f is the density of the fluid, g is gravity acceleration, k_n is the normal stiffness of the fracture, e_v is the void aperture of the fracture and C_f is the compressibility of the fluid. Doe and Geier (1990) argue that for reasonable magnitudes of stiffness and aperture the influence of the compressibility of water will be negligible. This is checked and confirmed in Thörn (2012) for the range of stiffness and hydraulic aperture that is relevant to the experiments in Publication III.

Transmissivity for a rectangular laboratory fracture sample can be evaluated in accordance with Darcy's Law as the specific capacity Q/dh with fracture length, L , and width, W , taken into account, (20).

$$T = \frac{Q \cdot L}{dh \cdot W} \quad (20)$$

For an in situ test of a borehole section, the transmissivity of the section can be calculated using Moye's formula (21) (see e.g.(Gustafson 2012)).

$$T = \frac{Q}{2 \cdot \pi \cdot \Delta h} \cdot \ln\left(\frac{L}{r_w}\right) \quad (21)$$

Where Q is the flow, Δh is the head change, L is the length of the section and r_w is the radius of the borehole.

For a section length that is short in relation to the fracture intensity, it is reasonable to assume that there will be one fracture in the section that is described by means of transmissivity. Where this section length to fracture intensity rule of thumb does not hold, it is still reasonable to assume that a large proportion of the flow originates from one single fracture. Gustafson (2012) states that the Pareto distribution has been found to fit transmissivity data well. This implies that for a packer interval with a few fractures, the most transmissive one will always be in the same order of magnitude as the total flow to the interval.

2.5.3 Tortuosity and channelling

Straight flow of water through a fracture only occurs if the surfaces are smooth and not in contact. In the case of rough fractures with contact points, the flow takes place around the contacts. The forced bending of streamlines is called tortuosity and is a measure of the length of a bent streamline in relation to a straight streamline (Hakami 1995).

To some extent, all fractures have wider and narrower parts of the aperture. In the wider parts, the flow velocity is higher, which is termed channelling (Hakami 1995). The effect of channelling is more or less prominent depending on the correlation between the surfaces. Channelling is also more prominent with regard to fracture systems since fractures with a larger aperture and intersections between fractures will act as channels (Hakami 1995).

2.5.4 Hydraulic aperture

The ability of a fracture to transmit water can be expressed as a hydraulic aperture. The hydraulic aperture is the spacing between two smooth parallel plates that enables the same amount of water to be transmitted. The cubic law (22), presented by Snow (1968) (see e.g. Gustafson (2012)) is a description of the flow between smooth, parallel plates.

$$T \frac{\rho_w \cdot g \cdot b^3}{12 \cdot \mu_w} \quad (22)$$

Where ρ_w is the density of water, g is gravity, b is the hydraulic aperture and μ_w is the viscosity of water. Witherspoon et al. (1980) examined the validity of the cubic law for fractures under stress and found it valid both for a case with contact points under stress and fractures held open. The validity under different conditions has been further discussed and scrutinized, and there are other models available to describe flow in fractures (Rutqvist and Stephansson 2003).

Zimmerman and Bodvarsson (1996) sought to find a way to describe the hydraulic aperture in a more correct way than the cubic law, which is based on the Navier-Stokes equations. The Hele-Shaw equations were used instead. A correction factor for contact points was found. They concluded that roughness would reduce the hydraulic aperture below the value of the mean aperture.

The effect of tortuosity is also addressed in Zimmerman and Bodvarsson (1996), which includes a discussion about a correct way to describe the shape of contact points. A description based on chessboard-like squares is used, which for a low concentration of contact points concurs with a description based on circular contact points. Each square either has an aperture of 0, with a probability of c , or an aperture of h_0 , with a probability of $(1 - 2c)$. A percolation limit, when the flow is completely obstructed, is present in this description ($c = 0.5$). The expression of hydraulic aperture, h_H , achieved by Zimmerman and Bodvarsson (1996) can be written as (23). It takes into account the arithmetic mean of aperture, $\langle h \rangle$, the standard deviation of aperture, σ_h^2 , and the contact area.

$$h_H^3 = \langle h \rangle^3 \left[1 - \frac{1.5\sigma_h^2}{\langle h \rangle^2} \right] (1 - 2c) \quad (23)$$

2.5.5 Hydraulic experimental methods

Unless stated otherwise, this section is based on Gustafson (2012). There are a number of investigation methods that describe the hydraulic properties of the rock mass. Test pumping means that water is pumped out of an entire borehole, or a section of the borehole, over a long period of time: in the order of days. The level of water in the borehole is monitored. Observations of pressure changes can also be made in other nearby boreholes; either for their entire length or specific intervals. This type of test is referred to as an *interference test*. If both pumping and observation boreholes are core-drilled, it is possible to identify and test the hydraulic properties of isolated fractures or fracture zones.

Packer tests, or water pressure tests, refer to injection of water between the rubbers of a double packer or from the rubber of a single packer to the bottom of the borehole. Pressure, volume and time are logged and from this transmissivity, storativity and skin factor can be evaluated.

Both pumping and injection tests require pumping of water. In the case of highly permeable formations, the quantities of water could be inconvenient to handle. In such cases a feasible method is *slug testing*, where a fairly small volume of water is removed instantaneously from the borehole, and the subsequent pressure recovery is logged (Rosberg 2010).

Weir tests can be conducted in tunnels, where a wall is built tight to the tunnel floor. The wall acts as a small dam and the flow across a weir in the dam can be measured to assess the natural inflow into a section of the tunnel. Natural inflow can also be measured in boreholes. The *Posiva Flow Log*, PFL, is an advanced instrument that can measure the inflow into 0.5 m sections of a borehole. This can be done incrementally to produce the inflow for individual fractures. Both inflow tests in boreholes and water pressure tests can be evaluated using Moye's formula (21). *Pressure build-up tests* are conducted by pumping or opening a borehole or borehole section and closing it while the pressure recovery is measured. This method is advantageous since it is easier to produce stable data when there is no flow in the borehole.

2.6 Hydromechanical description of fractures

The hydromechanically coupled description of fractures has been dealt with in the reviews by, for example, Rutqvist and Stephansson (2003), Zimmerman and Main (2003) and Jing and Stephansson (2007). Several models – empirical, analytical and numerical – are summarised in these reviews, presented by a host of researchers over the last four decades or so. The description here relies mainly on a couple of

relevant experiments as well as the JRC-based models by Barton (Barton 1982; Olsson and Barton 2001) and the work relating to fluid injection in boreholes by Fransson (Fransson et al. 2010; Fransson 2009; Fransson et al. 2007). Hydromechanical couplings can be subdivided into four classes, two direct, and two indirect (Wang 2000).

1. Direct solid-to-fluid; a change in applied stress changes the fluid pressure or fluid mass
2. Direct fluid-to-solid; a change in fluid pressure or fluid mass changes the volume of porous medium
3. Indirect solid-to-fluid; applied stress changes the hydraulic properties
4. Indirect fluid-to-solid; a change in fluid pressure changes the mechanical properties.

The direct couplings above are most influential in soft and low-permeability rocks and soils, while the indirect couplings apply more to fractured rock. The tests performed in Publication III could be designated *hydrostatic compression tests* (Heiland 2003), and fit into class 3, as seen in Rutqvist and Stephansson (2003). The experiments in Publications I-II fit into class 4, where a change in fluid pressure affects the mechanical properties.

Hakami and Larsson (1996) performed flow tests and measured the mechanical aperture for a 45 cm natural fracture sample in granite, which under a confining pressure of 0.45 MPa had a mechanical aperture of 360 μm and a hydraulic aperture of 250 μm . In experiments on epoxy replicas of natural fractures by Hakami and Barton (1990) the ratio between mean aperture and hydraulic aperture was found to be in the range 1.1 - 1.7, with a mean aperture of 100 - 500 μm .

Iwano (1995) conducted stress-flow experiments on three fractures in Kikuma granodiorite, one natural joint, one tension joint and one sawn and grit surface. The cores were \varnothing 50 mm and h 100 mm. The procedure was 1) Measurement of surface geometry and derivation of aperture geometry, 2) Cyclic stress-flow experiments using deformation measurements in a triaxial cell with confining pressures up to 20 MPa, 3) Repetition of 1. In all the experiments performed by Iwano (1995) a large hysteresis of the transmissivity was observed.

Barton (1982) proposed a relationship between hydraulic aperture, e , and mechanical aperture, E , which was later updated in (Olsson and Barton 2001) for different levels of shear displacement, u_s , related to the peak shear displacement, u_{sp} , which are valid for $E \geq e$ (28 and 29) The relationship between normal and shear

displacement (30) use a mobilised dilation angle, d_{nmob} (31). The basis for these expressions is a series of experimental data.

$$e = \frac{E^2}{JRC^{2.5}} \quad \text{for } u_s \leq 0.75u_{sp} \quad (24)$$

$$e = \sqrt{E} \cdot JRC_{mob} \quad \text{for } u_s \geq u_{sp} \quad (25)$$

$$\Delta u_n = \Delta u_s \tan d_{nmob} \quad (26)$$

$$d_{nmob} = \frac{1}{M} JRC_{mob} \log_{10}(JCS/\sigma_n) \quad (27)$$

From (27) it can be discerned that fresh (high JCS) and rough fractures (high JRC) give rise to a large mobilised dilation angle. An example of fractures expected to fulfil that is tensional fractures.

Fransson et al. (2010) developed a model for describing deformations during grouting in situ, based on fracture volume change. An initial hydraulic aperture needs to be determined using a hydraulic test. The grouting procedure needs to be logged with pressure, grouted volume and time. The flow dimension of the grout can be determined using this pVt -data. Based on the type of grout, the penetration length can be calculated for each time step. This enables calculation of the area under grout overpressure. Assuming a cone-shaped profile of the grout overpressure gives a measure of the force acting on the fracture. This, together with calculation of initial volume of the fracture compared to the actual grout take, gives a measure of fracture stiffness.

Data from interference tests investigating deformation zones at Äspö HRL and the nearby study area Laxemar were compiled by Rhén et al. (2008) and were presented as a relationship between transmissivity, T , and storativity, S (32).

$$S = 0.0109 \cdot T^{0.71} \quad (28)$$

Fransson (2009) linked (28) with the expression of storativity to stiffness, (19), which results in a description of fracture normal stiffness from the transmissivity (33), evaluated from a hydraulic interference test. Furthermore, this is linked to the cubic law, (22) to give a relationship between hydraulic aperture and fracture normal stiffness.

$$k_n = \rho_f \cdot g \cdot \left(0.0109 \cdot \left(\frac{\rho_f \cdot g \cdot b_h^3}{12\mu} \right)^{0.71} \right)^{-1} \quad (29)$$

Fransson (2009) compiled in situ data from the surficial limestone laboratory in Coaraze in France, the Röda Sten Rock Laboratory in Gothenburg, the Rock Mechanics Laboratory in Luleå, Äspö HRL and the Underground Research Laboratory in Canada (Figure 14). Normal stiffness from the experiments was plotted against hydraulic aperture and in the cases of RML, Luleå and Äspö HRL, data were in the form of hydraulic normal stiffness, i.e. calculated from changed hydraulic aperture. The relationship (29) was included in Figure 14 as a red line and with an offset of plus/minus one order of magnitude. The relationship is expected to be valid for fractures under low effective compressive stress, with limited fracture infilling and small amounts of permanent deformation.

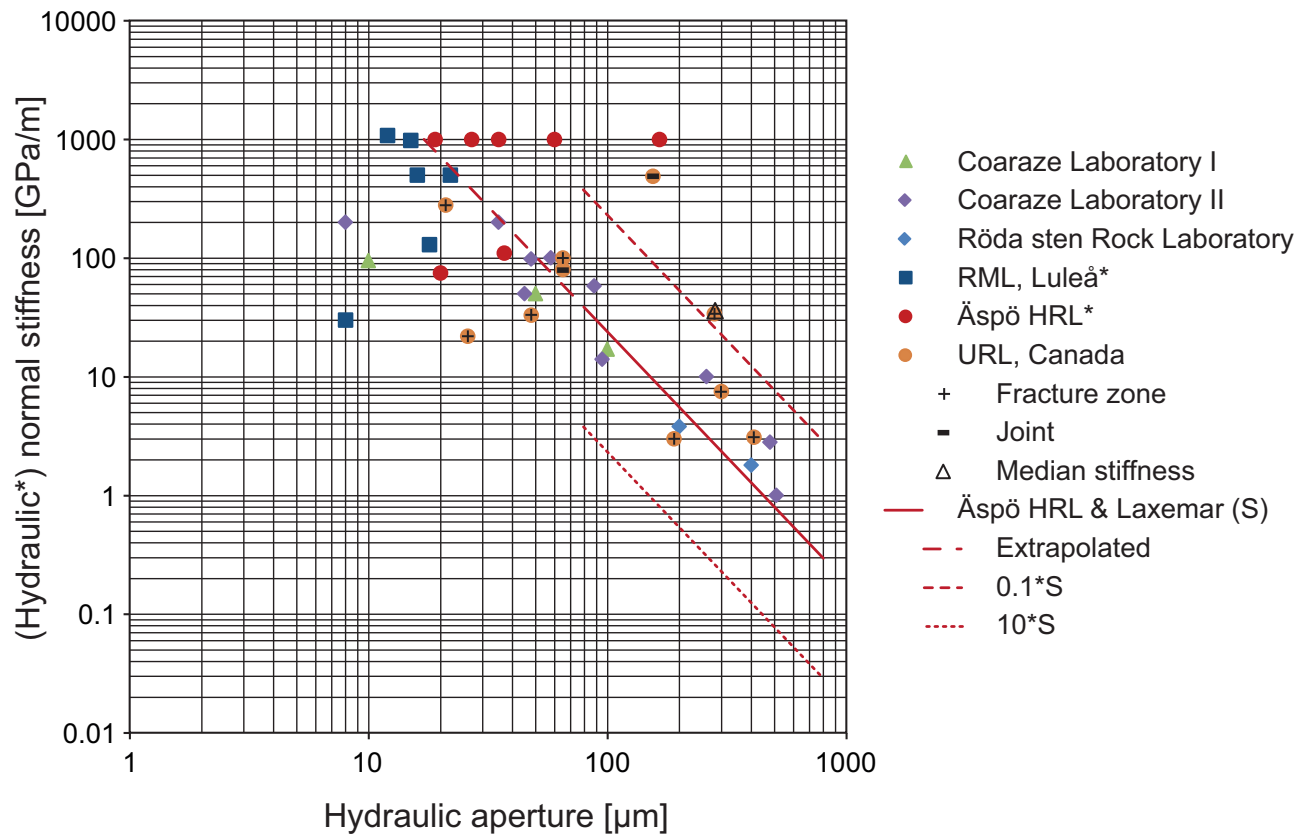
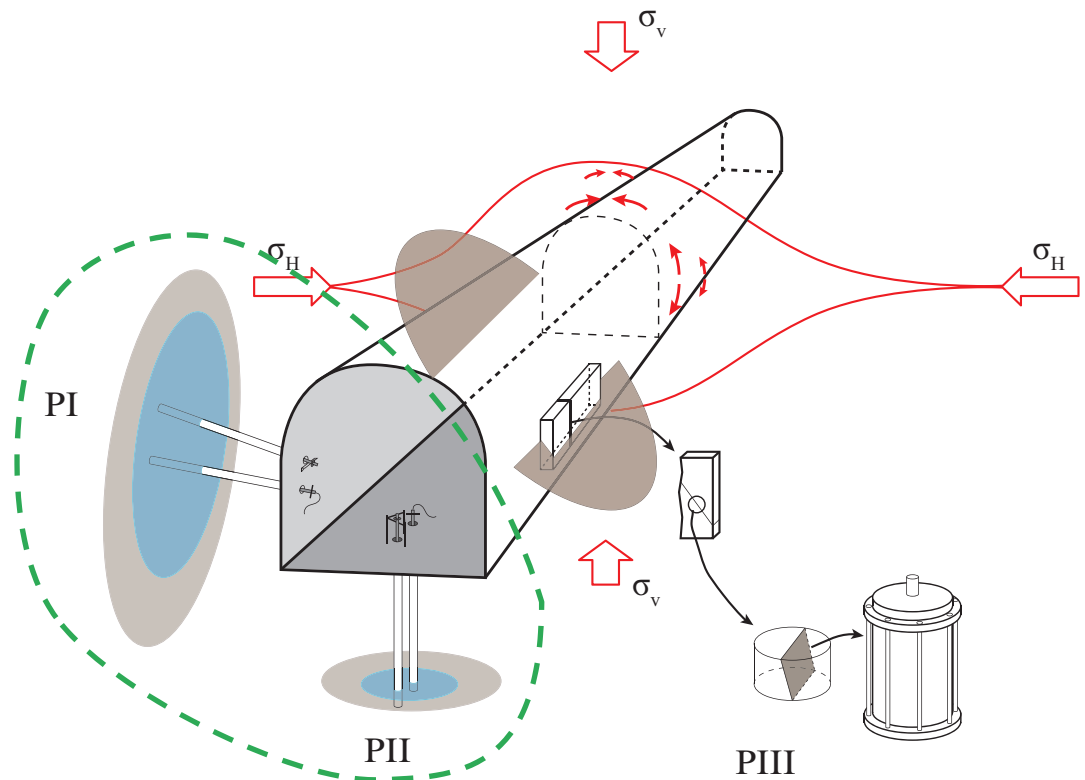


Figure 14: Compilation of stiffness to hydraulic aperture from (Fransson 2009).

3 HYDROMECHANICAL EXPERIMENTS IN SITU (PUBLICATIONS I & II)



Publication I and Publication II both cover in situ experiments. The measurements in Publication I were carried out in the Hallandsås Tunnel within the scope of a master's thesis (Runslätt and Thörn 2010). Measurements were conducted in the tunnel wall during hydraulic testing and grouting as part of a post-grouting scheme (Figure 15). The working hypothesis was that substantial deformations were expected for the stress relief part in the tunnel wall, since the grouting overpressure was close to the low rock stress (see section 2.2). With the heavily fractured rock mass, hydraulic contact between boreholes was expected and this was verified by means of initial hydraulic testing.

The measurements presented in Publication II were conducted in the TASO Tunnel at the Äspö HRL as part of the Bentonite Rock Interaction Experiment, BRIE (see Figure 16). The in situ stresses at this site are greater than in Hallandsås and the rock mass is significantly less fractured. Here, measurements were made in the tunnel floor on two occasions: December 2010 and September 2011. With the higher

levels of stress in TASO and with testing taking place in the floor, small or no deformations were expected. Some interesting fractures were identified through hydraulic testing within the BRIE project and were the target of the deformation measurements. Drilling of some borehole sections produced pressure responses in adjacent boreholes, which is evidence of hydraulic contact. With mapping of the cores from the boreholes, individual fractures could be identified as being responsible for the contact. Unfortunately, BIPS logging and analysis did not produce correct orientations and have to be further considered. Therefore, the results of the geometric modelling in Publication II do not reflect the actual situation at TASO, but the general conclusions of Publication II still apply.

3.1 In situ experimental design

A dual-borehole set-up for measuring deformation in one borehole as an effect of a nearby borehole being pressurised was presented in (Runslätt and Thörn 2010) and Publication I. An ordinary single packer was placed in one borehole and the measurement equipment in a nearby borehole (Figure 15). Previous hydraulic characterisation had proved the boreholes to be in hydraulic contact. Deformation was measured as elongation of the rock mass, i.e. deformation of fractures between an anchor and the rock surface in the tunnel, connected by a steel pipe (see Figure 15). The measurement borehole was at atmospheric pressure.

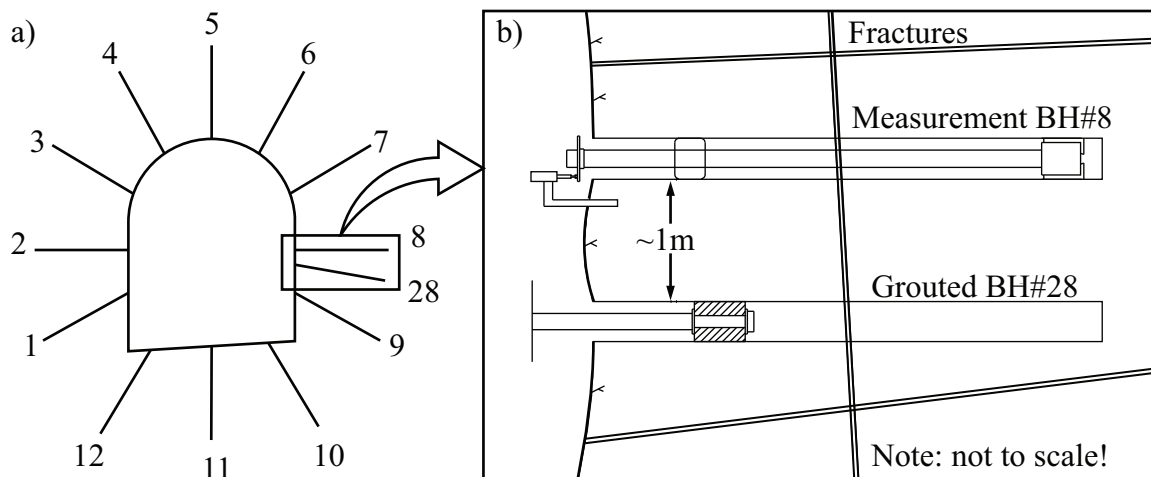


Figure 15: A drawing of the experimental set-up used in Hallandsås, Publication I. The measurement borehole, No.8, was inclined slightly upwards. Note the borehole geometry for reference to the results in Table 3. (Figure from Publication I).

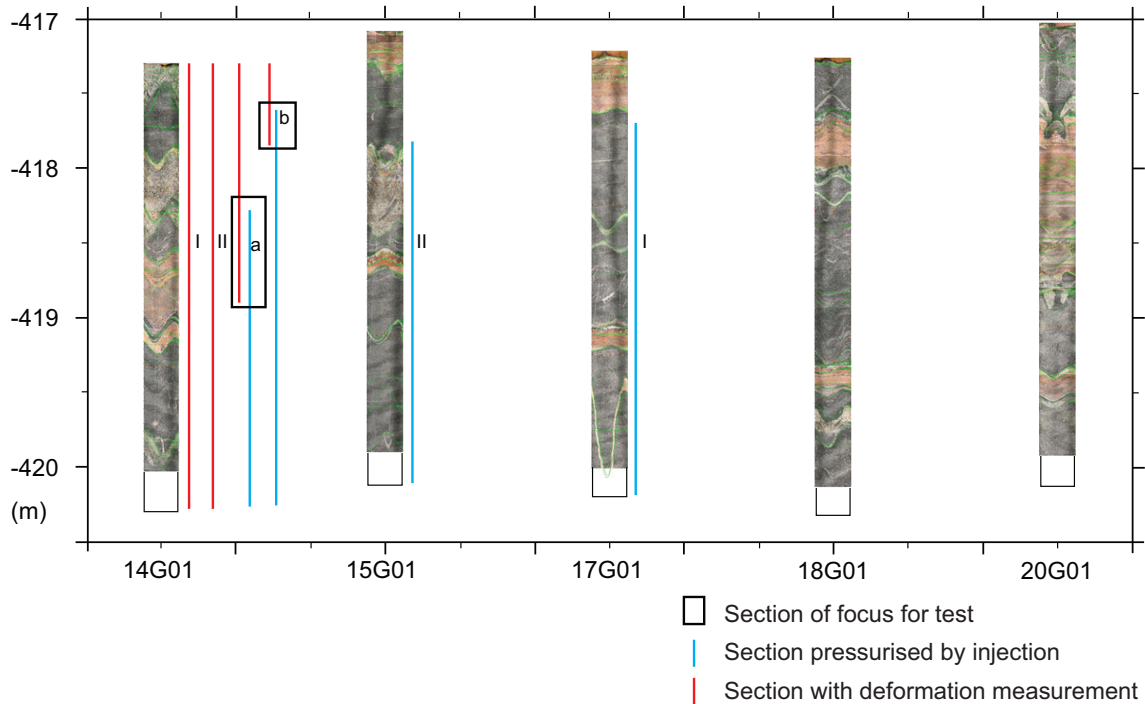


Figure 16: The primary boreholes in TASO, represented by borehole photographs (Sicada 2013). The sections of the boreholes that were pressurised by the injection, and subject to deformation measurements are marked.

Publication II is based on two sets of measurements in TASO at the Äspö HRL. On both occasions, the same boreholes in the tunnel floor were used although the equipment was updated, see Figure 17. The first round of measurements in Publication II used the set-up introduced in Publication I, while the second round used a single-borehole set-up, Figure 17 and Figure 18. The plug (B) was a last-minute adjustment of the equipment that caused undesired deformations in the equipment, making interpretation of the results difficult. In a third round of (unpublished) measurements in TASO this issue had been resolved.

Measurements (1)-(4) represent: (1) interval of deformation measurement; (2) pressurised interval with deformation measurement; (3) length of packer, adjustable c 0.5-2.7 m; (4) length of deformation measurement pipe 1.1-4.6 m. Letters A-I represent: A. deformation sensor, B. plug, C. reference plane, D. seal, E. injection connection, F. packer tightening nut, G. packer rubber, H. deformation measurement pipe, I. anchor.

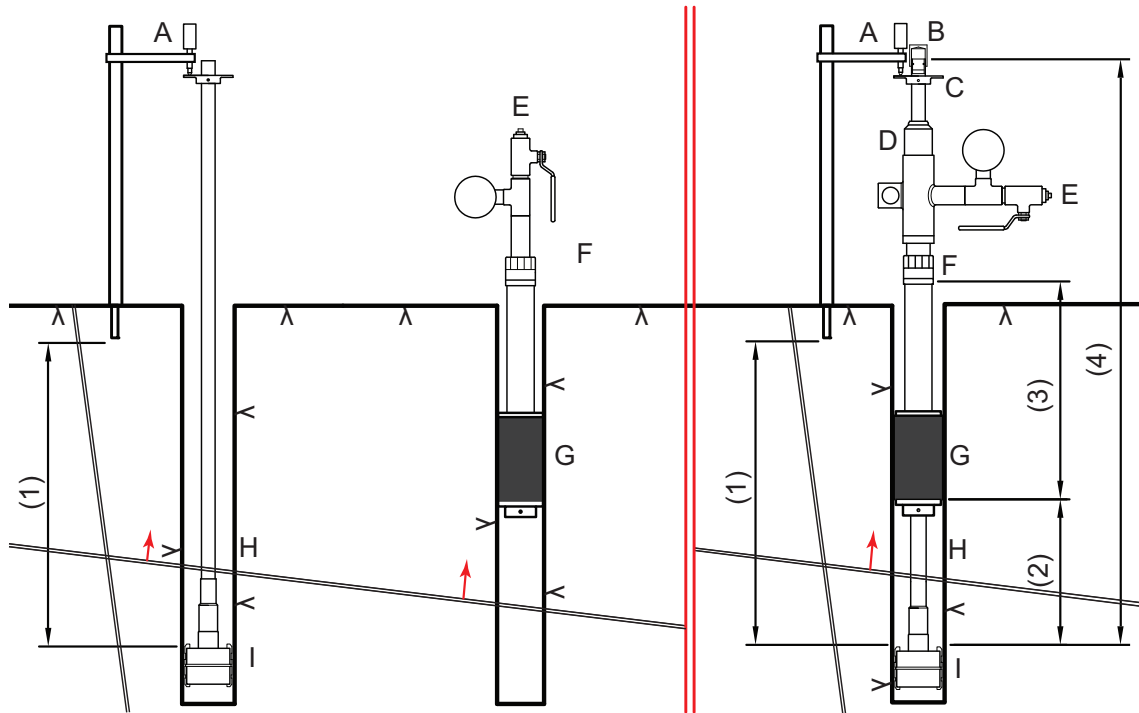


Figure 17: Left and centre: Equipment for the December 2010 tests. Right: Drawing of the measurement equipment for the September 2011 test series. (Figure from Publication II).



Figure 18: Left: Measurement borehole in the Hallandsås measurement. Centre: Measurement borehole in the first round of TASO measurements, note the concrete slab on the floor. Right: Combined measurement/injection borehole in the second round of TASO measurements, conducted after the concrete slab and gravel (c 0.6 m) had been removed.

3.2 Results

The testing sequence of the Hallandsås measurement started with a water pressure test in BH8 (see Figure 15), with pressure logging in BH28, in order to determine if there was contact between the boreholes. Four injection tests (WPT 1-4) were then performed with injection in BH8. WPT1-3 had the deformation anchor attached at a depth of 4.5 m while WPT4 had the anchor attached at 2 m. The three subsequent measurements during grouting had the anchor attached at 4.5 m. Deformation values from the Hallandsås measurements (Δa) (Publication I) can be found in Table 3. Permanent and resilient deformations were recorded for most of the tests. Permanent refers to the part that did not return after the pressure was released and resilient refers to the rest of the deformation up to the maximum value.

From the Publication I deformation data and the injection over-pressures, fracture stiffness was evaluated in accordance with (12) (Table 4). In the WPTs, the deformation curves showed two more or less marked stages of deformation; one initial with a lower rate of deformation and a subsequent stage where the rate of deformation was higher. Stiffness was evaluated separately for these stages, which is represented as pressure, deformation and stiffness intervals in Table 4. Definition of the deformation stages was not done in an entirely strict way and in some cases this resulted in overestimation of the later stiffness behaviour. These values are marked with an asterisk (*) in Table 4.

Table 3: Permanent and resilient mechanical deformations, Δa , of the Hallandsås measurements.

Injection test	Deformations in BH8						
	WPT1	WPTs in BH28			WPT4	Grouting	
WPT2		WPT3	WPT4	BH9		BH28	BH7
Distance to BH8	1	1	1	1	4	1	4
Permanent Δa [μm]	14	0	48	11	19	18	0
Resilient Δa [μm]	39	31	125	42	17	37	30
Total Δa [μm]	53	31	173	53	36	55	30

Table 4: Evaluated fracture stiffness from the Hallandsås experiments. The evaluation was divided into two stages; one initial stage with a stiffer behaviour and one subsequent stage, identified from a more or less marked change in the deformation curve after which the deformation rate was higher and the stiffness lower. This is represented as a span in the table.

Test	Δa [μm]	Δp [MPa]	$k_n^a = \frac{\Delta p/3}{\Delta a}$ [GPa/m]
WPT1	28 - 53	0.8 - 1.0	9.6 - 6.5
WPT2	5 - 25*	0.3 - 0.8	23 - 11*
WPT3	4 - 125*	1.0 - 1.0	79 - 2.6*
WPT4	5 - 32*	0.6 - 0.8	37 - 8.6*
G-BH9	27	0.4	4.9
G-BH28	45	0.9	6.6
G-BH7	25*	1.4	19

*Value where Δa is underestimated, rendering an overestimation of k_n^a .

The in situ experiments presented in Publication II were targeted at certain sections of the boreholes where previous hydraulic testing had identified contact between the boreholes. Table 5 shows the borehole that was injected through a single packer, i.e. from the specified packer depth down to the bottom of the hole, approximately 3 m. The table also shows the borehole where deformation measurement took place and the position of the anchor. Deformation measurement took place from the anchor depth up to the surface of the borehole. Tests I and II refer to the first measurement occasion, i.e. the dual-borehole set-up, while A and B refer to the single hole set-up (see positions in Figure 16). More measurements were conducted on this occasion but due to the previously mentioned difficulties with the plug on the pipe, the two most reasonable sets of results are presented. Results in terms of measured deformation, change in hydraulic aperture in the injection borehole and evaluated fracture stiffness are presented in Table 5.

Table 5: Test conditions – selected measurements in TASO, Publication II, see Table 6 for results.

Test	Injection borehole [KO00...]	Packer depth [m]	GW pressure [MPa]	Pressure sequence relative GWp, Δp [MPa]	Measurement borehole [KO00...]	Anchor depth [m]
I	17G01	0.5	1.2	0.2; 0.4; 0.6; 0.4; 0.2	14G01	2.93
II	15G01	0.75	0	0.2; 0.4	14G01	2.93
A	14G01	1.0	0.207	0.2; 0.4; 0.6; 0.4; 0.2	14G01	1.60
B	14G01	0.35	0.011	0.2; 0.4; 0.6; 0.4; 0.2	14G01	0.55

Table 6: Initial hydraulic aperture (from the first pressure step), change in hydraulic aperture, Δb (at the highest pressure step), measured deformation, Δa , and the fracture normal stiffness estimated from these. Reference can be made to Table 5 to identify the positions of the tests.

Test	$b_{initial}$ (borehole) [μm]	Δb (borehole) [μm]	Δa (borehole) [μm]	Δp [MPa]	$k_n^b = \frac{\Delta p/3}{\Delta b}$ [GPa/m]	$k_n^a = \frac{\Delta p/3}{\Delta a}$ [GPa/m]
I	10 (17G01)	0 (17G01)	0 (17G01)	0.6	Inf.	Inf.
II	130 (15G01)	3 (15G01)	3 (15G01)	0.4	40	40
A	3 (14G01)	5 (14G01)	Uncert.(14G01)	0.6	40	n/a
B	16 (14G01)	3 (14G01)	Uncert. (14G01)	0.6	70	n/a

3.3 Reliability of in situ methods and results

Publication I concluded that the method was robust. In Publication II, some issues were raised concerning the set-up. Below is a discussion of the uncertainties of the in situ method.

Having a steel pipe a few metres in length and measuring exact deformations with the pipe raises the question of temperature elongation and mechanical stiffness of the steel material. In the case of Publication I, the pump flow was significant although the water had been inside the tunnel for quite a long time and had a temperature close to that of the rock. Furthermore, the measurements were conducted in spring, when the outside and tunnel temperatures are fairly close to that of the rock. In the case of the measurements in Publication II, the flow rate was very small and the water was the same temperature as the tunnel. Temperature elongation cannot be an issue in this case. For all the measurements, the logging started after some time, thus giving the pipe time to adjust to the borehole temperature.

As regards the stiffness of the pipe, in Hallandsås it was centred in the borehole using Teflon bushings, causing minimal friction. The pipe can thus be regarded as stiff. In the first set of measurements in TASO, the pipe was vertical, with a loose brass ring attached to the surface rig to keep it in place. Friction can also be ignored here. The second set of TASO measurements had the single-hole set-up, where a pressure seal was needed between the packer and the pipe. Manual testing in unpressurised conditions suggested low friction but this was not tested under pressurised conditions. If friction between the seal and pipe was an issue during single-hole testing, this ought to show up in a systematic way for all experiments but this was not the case. This suggests that the pipe was not affected mechanically on the outside in this case either.

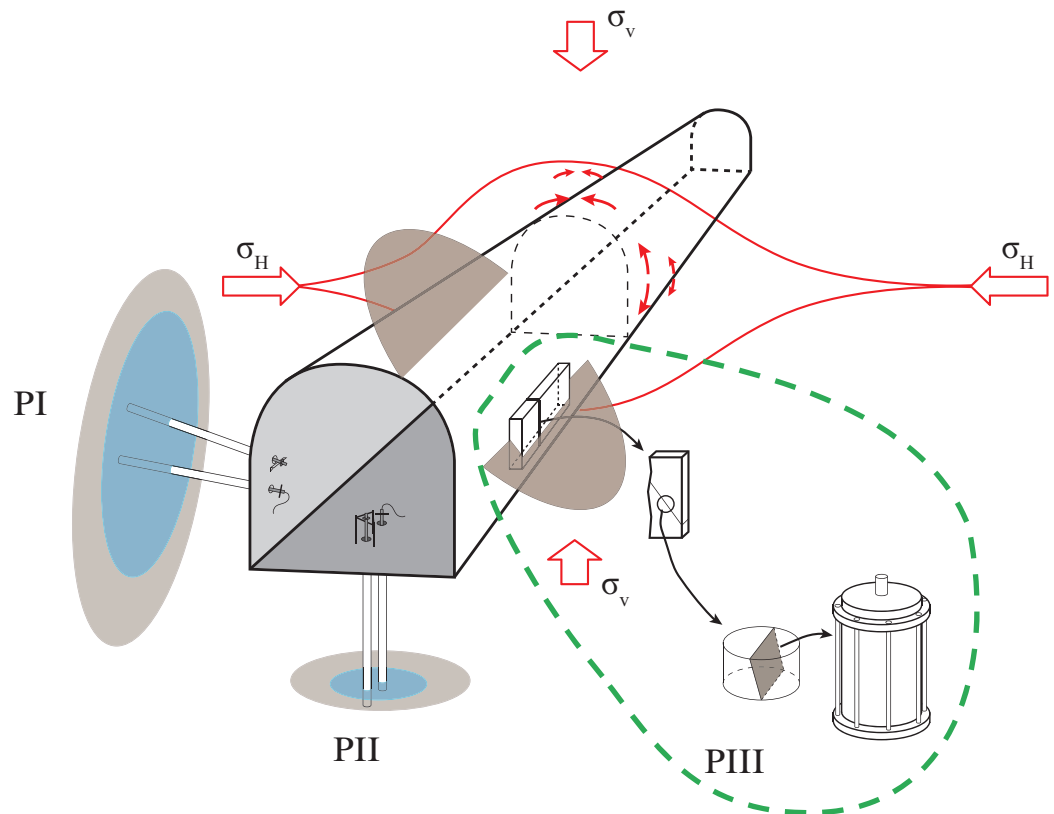
The anchor was installed firmly and the pipe was tugged slightly after installation for verification. At Äspö (Publication II), the anchor was installed in cored boreholes and in sound rock at intact sections. For Hallandsås (Publication I) the anchor was installed in percussion-drilled boreholes in heavily fractured rock. However, a sub-horizontal testing borehole and an anchor design that allows water to flow past the anchor would make it unlikely that the anchor moved during measurement.

As regards the surface part of the set-up, i.e. the rig to which the deformation meters were attached, in Publication I it was bolted onto the wall shotcrete, well away from external disturbance. For the first round of measurements in Publication II, the set-up was devised for bolting into the rock close to the borehole, through the concrete floor slab on top of the gravel that was in the TASO Tunnel at the time. The set-up was sensitive to touching and the borehole was placed centrally where there was least space (see darker “walking path” in Figure 18, centre). Consequently, the rig was accidentally kicked and stumbled over a number of times, most of which were observed and noted. A few disturbances in the results were interpreted as accidental even though they were not noted.

Electronic logging of deformation at 1 s resolution was successful in the Hallandsås Tunnel although in TASO disturbance in some form created signal noise that was greater than the observed deformations. Here the results rely on the back-up logging system – a camera on a tripod – with manual photographing of a mechanical 0.001 mm deformation meter. The camera clock was synchronised with the computer that was logging other data in the tunnel. Data was extracted by means of macro-reading of the time stamp for each picture and manual reading of the deformation meter value in the picture. This was slightly tedious but worked well and saved time and attention in the tunnel.

The method allows measurements axially along a borehole, and consequently it is only able to record the axially aligned component of any given deformation, regardless of the type of deformation.

4 HYDROMECHANICAL EXPERIMENTS IN THE LABORATORY (PUBLICATION III)



The laboratory experiments (Publication III) were conducted during early 2011 and were devised to determine both hydraulic and mechanical aperture changes due to changing confining pressure on the core sample. The experiments were conducted with cell pressures up to 2.5 MPa, which roughly corresponds to the low-stress situation near the wall of the tunnels, TASS and TASQ. Samples were selected from the ones used in Ericsson et al. (2009) with the aim of achieving a variety of apertures although with the simplest fracture geometries and as little previous testing as possible. One sample from TASS (PS0039061) that had been subject to cyclic testing was used to try out the method but at lower confining pressure cycles. This worked well and two samples from TASS (PS0039023 and PS0037053) and one from TASQ (AB1AB2) were tested with the final cell pressure sequence.

4.1 Development of lab equipment

A permeameter cell for testing cylindrical samples with a height of about 100 mm and a diameter of 190 mm and with sub-vertical fractures, was built and used by (Ericsson et al. 2009). In Publication III, the permeameter cell was updated with a small deformation sensor (Figure 19). The updated procedure enabled measurement of fracture flow and simultaneous fracture mechanical opening/closure measurement. Measurements were conducted on four samples at stepwise load cycles of isotropic pressure inside the cell. The maximum pressures for the cycles were 1.0, 1.5, 2.0 and 2.5 MPa.



Figure 19: A cutaway photomontage of the permeameter cell used in Publication III. For size reference, the specimen is 190 mm wide and 100 mm high. The valve to the lower left is the water inlet, which is connected to the bottom plate (1) where the water is distributed. Water is collected in the top plate (4) and led through the pipe out of the cell, where the flow is measured (Figure modified from Publication III).

The output from the experiments was 1) a flow rate for each pressure step, established through three flow readings, logging the time to fill a measurement container (2-100 ml), and 2) the displacement across the fracture at the point of the deformation meter. All logging was done using the same computer, which gives automatic time synchronisation and greatly simplifies data processing; a lesson learned from work in Publication I. At each pressure step, the initial deformation was followed on a screen and given some time to stabilise before the flow readings commenced. The flow readings showed a gradually decreasing value and seemed to approach a stable value asymptotically. The third reading was therefore used for each pressure step.

4.2 Results

Hydraulic aperture, evaluated using the cubic law and mechanical deformation, both as a function of confining pressure, was the experimental results of Publication III, co-plotted in Figure 20. Note the different scale bars in the figure. Hydraulic aperture, b , is given as an absolute value below the diagrams, decreasing to the right in order to fit the mechanical deformation, Δa , on the top axis, where the convention is that closure is positive. Note also that only PS0039061 has a $\Delta a/b$ -ratio of 1:1. The ratio has been set differently between the graphs to enable a direct comparison between hydraulic and mechanical responses. It is evident that PS0037053, PS0039061 and AB1AB2 have similar responses while PS0039023 shows the same type of hydraulic hysteresis as the other samples but with an elastic mechanical response.

Both hydraulic and mechanical behaviour were evaluated in terms of fracture normal stiffness. The stiffness of each pressure step for the samples was plotted against the hydraulic aperture (Figure 21). The differing behaviour of the samples was put into a conceptual description that exemplified the measured behaviour using type fractures, subject to different amounts of translation under low stress.

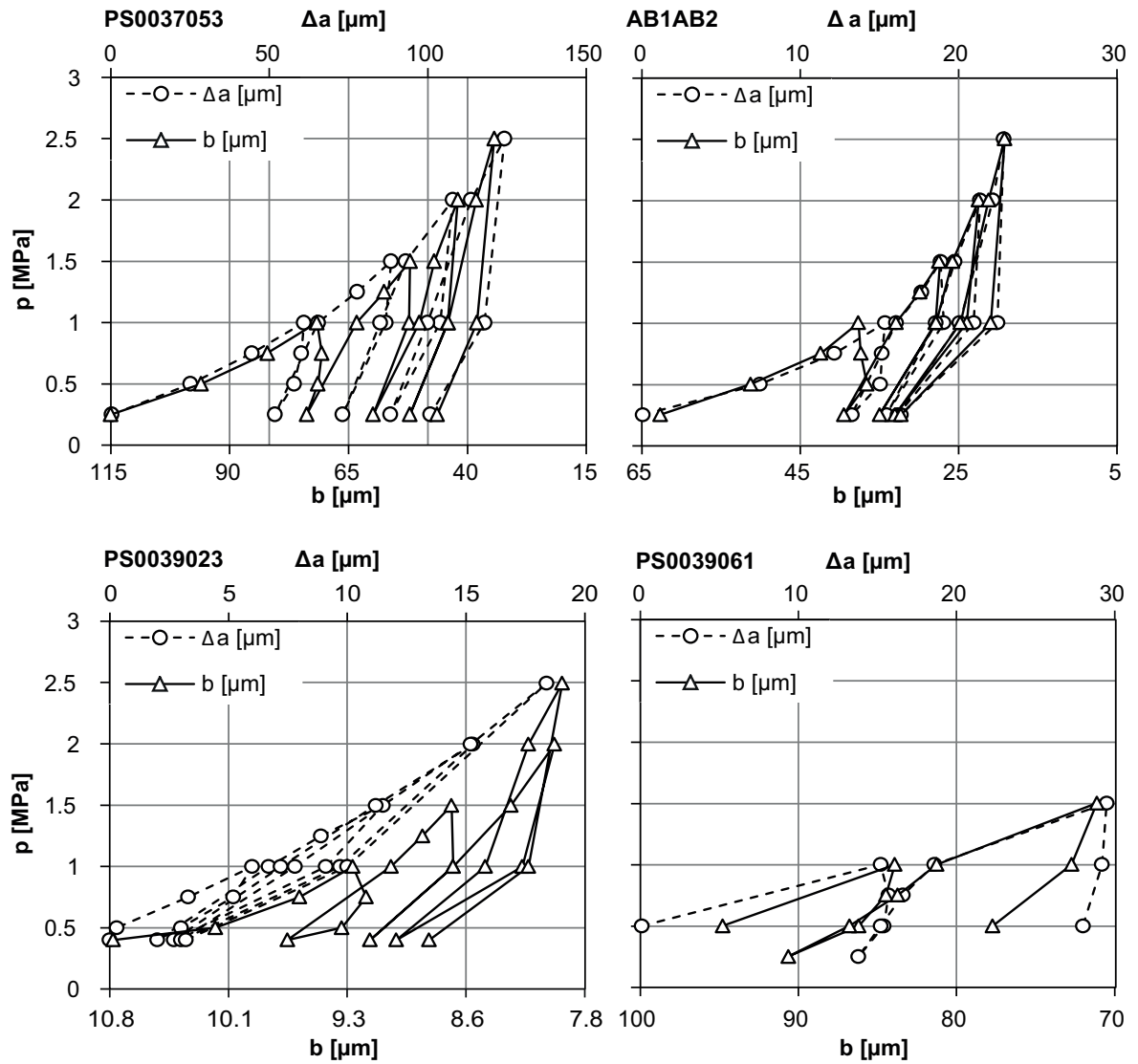


Figure 20: Hydraulic aperture, b , and mechanical deformation, Δa , from the experiments. Note the different scales of the b and Δa axes and between the graphs. (Figure from Publication III).

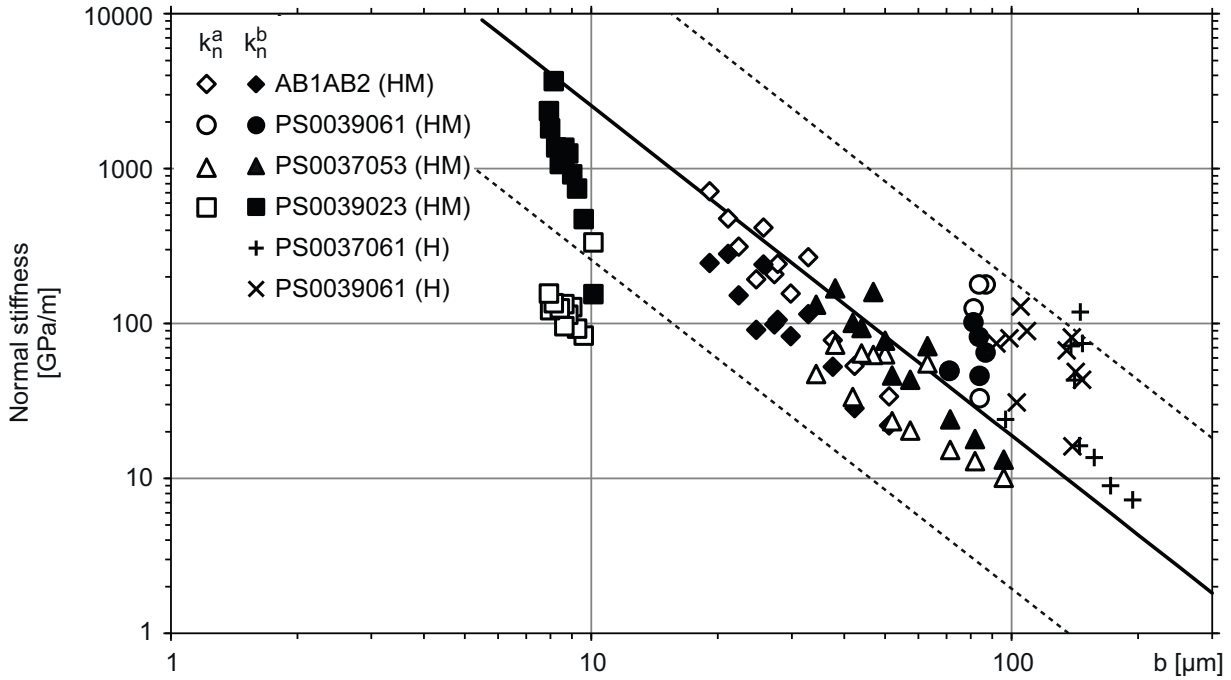


Figure 21: Measured stiffness from experiments. The lines represent equation (33) \pm one order of magnitude. Three types of behaviour are identified and further discussed in chapter 6 (Modified from Publication III).

4.3 Reliability of laboratory method and results

Larsson (1997) derived the pressure over a fracture through a biaxially loaded cylindrical rock sample to be homogeneous normal pressure equal to the cell pressure. This derivation is also valid for three-dimensional hydrostatic loading since the volumetric stress over the fracture is equal to the cell pressure. The effect of the water pressure inside the fracture is insignificant for most samples since this pressure is about 0.65 m water column and significantly lower than the cell pressure. However, caution may be needed for the lowest confining pressure steps of the samples tested at $dh = 35$ m. Iwano (1995) conducted triaxial testing of rock cores and concluded that it did not seem to make a difference if the stress was applied as normal stress or confining stress. Calculations of the results therefore used the confining pressure step change as a numerator in (12) i.e. normal stress change.

The chosen stress range for the experiments, 0-2.5 MPa, is based on a basic distinct element analysis of the stresses in the area of the sawn-out slot (Ericsson et al. 2009) using Examine 2D (Rocscience 2010) and assuming an idealised tunnel contour. Input was real stress data from the area of the TASS Tunnel as well as the size and orientation of the tunnel. The three induced stresses were estimated to be within 0-7 MPa in the rock volume of the slabs where the samples were taken. An estimate with positions and orientations of the specific sampled fractures and with an idealised tunnel contour also resulted in normal and shear stresses in the range 0-8

MPa. For the samples that were subject to cyclic testing, the normal and shear stresses were as follows: PS0037053 and PS0037061: 1-1.5 MPa; PS0039023: 4-8 MPa; PS0039061: 3-5 MPa. This type of estimate has not been made for AB1AB2 from TASQ.

The equations used for flow in fractures require laminar conditions. The experiment parameters were checked for turbulence according to (18) and were found to be well within the laminar regime.

At each pressure step, the flow value was measured three times. With a few exceptions, flow readings two and three were lower than the first one or two readings for each confining pressure step. The value of the third reading was used for further analysis, supported by the fact that the flow seemed to asymptotically approach a stable value.

A Monte Carlo simulation was performed on a dozen uncertainties regarding the measured test conditions and values (see Thörn 2012). Uncertainty was expressed in terms of the $\Delta b/\Delta a$ -ratio. The largest contribution to the variance, i.e. to the simulated total uncertainty was found to lie in assessing the representative time to fill the measurement cylinder, which is a consequence of the asymptotically stabilizing flow. Expressed in terms of $\Delta b/\Delta a$ -ratios of sample AB1AB2, the uncertainties for increasing-pressure steps were insignificant. For some of the decreasing pressures steps the uncertainty was large and in general the decreasing pressure steps were found less reliable (Thörn 2012).

The experimental set-up used one deformation transducer placed near the centre of the top surface. It was assumed therefore that no rotation of the sample halves occurred. To develop the equipment further, the addition of another one or two transducers on the bottom surface should be considered.

Sample PS0039023 was partially sealed although the extent is unknown. The evaluation of hydraulic aperture, however, is based on the entire width of the fracture trace across the sample. Hydraulic apertures evaluated from the open part of the fracture could be up to 5 μm larger.

The effect of sampling and handling must be addressed when conducting laboratory experiments. Here, the experiments are performed on real fracture samples with a true local surface geometry from the sampled fractures. It is not likely that the relative positions of the fracture halves were kept perfectly throughout two rounds of permeameter testing with handling and storage in between.

5 DISCUSSION

The discussion chapter is divided into two main sections. The first part deals with the generation and evolution of fractures up to the stage when a tunnel has been constructed. The second part deals with the current situation close to the tunnels and how this is affected by testing and sampling. The discussion regarding the measurement methods as such takes place mainly at the end of the publication chapters.

5.1 Geological history and resulting fracture geometry

The surface geometry of individual fractures has a significant impact on the hydromechanical response of the fractures and is governed by the geological history. One response, the stiffness, is highly dependent on the surface geometry and has been a particular focal point in this work. The stiffness of a fracture increases with the increasing area of contact between the surfaces. This can be achieved by existing contact points growing or the formation of new contact points. Growing points do not affect the tortuosity as significantly as if new contacts had been formed, since new contacts are expected to obstruct flow paths to a greater degree and thereby increase the tortuosity. Compare the behaviour of PS0037053 and PS0037061, represented as triangles and plus signs in Figure 23.

The growth of the contact area with an increased mechanical load across a fracture occurs in different ways depending on the matedness of the fracture. A distinction can be made between *mated* and *unmated* fractures. Unmated fractures have large apertures if the shearing occurred under low normal stress and mated, unsheared fractures have small, or ideally no aperture if they are in a compressional stress field, see Figure 23.

A *well-mated* fracture is likely to have a large number of small contact areas, points, and a small aperture, while an unmated fracture has fewer contact points and a larger aperture. If the shearing that unmates a fracture occurs under a sufficient amount of normal stress, some asperities in the fracture topography are sheared off. In Olsson and Barton (2001) (27) this is handled by introducing a damage coefficient in the denominator, M , which is set at 1 if shearing occurred under low stress, and 2 if shearing occurred under high stress; i.e. halving the dilation angle for high stress shearing. Assigning a smaller dilation angle means that the effect on transmissivity from shearing is smaller. Consequently, an unmated fracture sheared under moderate to high normal stress has few larger areas in contact, while a mated fracture has more numerous yet smaller areas in contact, given that they are under the same amount of normal stress. Cf. exemplified geometries in Figure 22.

The stress situation during fracture formation and subsequent reactivations affects the appearance of the fracture, which influences its hydromechanical behaviour. With knowledge of the stress history of a site, some general idea of the hydromechanical behaviour of individual fracture sets may be inferred.

The hydromechanical response of fractures close to tunnels is also dependent on the current rock stress situation in the near-field of a tunnel, which can be deduced from knowledge of the primary rock stresses or from measurement. In the redistributed stress field around a tunnel, parts of the periphery experiences stress concentration while other parts experience relief. With horizontal stresses being the largest, the stress relief part will be in the tunnel wall. Cf. stress modelling of TASS (Ericsson et al. 2009), which served as a basis for selecting the stress range for the laboratory work in Publication III.

Transmissivity is affected by shear movement differently for different fracture types. Tensional fractures may be too rough for shearing at all under a given level of shear stress but if they do shear under low compression, the effect on transmissivity is significant (a high dilation angle). Shear fractures have a lower dilation angle and the effect on transmissivity is not necessarily significant.

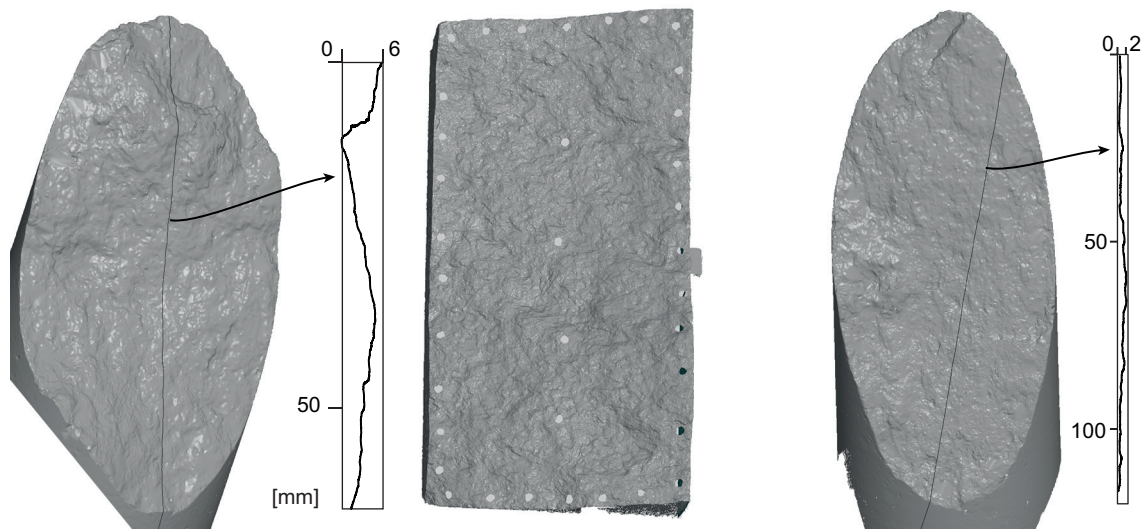


Figure 22: Examples of geometries of fracture surfaces. Left: Rough fracture from TASO. Centre: PS0039061 (100 by 190 mm). If shearing has occurred, it has probably been under low normal stress, since the geometry is still rough. Right: Sheared fracture (it visibly offsets a pegmatite vein). The flatness of the surface suggests that shearing occurred under high normal stress; 62 mm core sample from TASO.

5.2 Fracture geometry, present stresses and stress changes

In this thesis, laboratory and in situ experiments were used to show deformation and stiffness behaviour of fractures close to tunnels. The behaviour is presented in section 5.2.1: the stiffness relation to aperture, in this case the far more easily obtainable hydraulic aperture, and 5.2.2: the relationship between stiffness evaluated from changed hydraulic aperture and stiffness from measured deformations.

The bulk of the data set presented within this thesis comes from the laboratory experiments conducted in a controlled environment. The laboratory experiments were conducted on samples that can be described in their corresponding geological context, although too few samples were tested to draw general conclusions relating to the geological history of the site. More tested samples, including all prominent fracture sets and mineral fillings, would enable a better link to geological history. However, the general trend of low stiffness for large aperture fractures and high stiffness for low hydraulic aperture fractures has been captured in the experiments, cf. Fransson (2009).

The in situ experiments demonstrated deformation and stiffness behaviour in two significantly different geological settings; Hallandsås (low stress, high fracture intensity) and Äspö HRL (high stress, lower fracture intensity, at least outside the EDZ). The calculated stiffness from Hallandsås was lower than from the measurements at Äspö. A contributing factor to this difference is the stress situation, where the principal stresses at Äspö are roughly one order of magnitude greater than for Hallandsås.

5.2.1 Aperture-stiffness relationship

A selection of stiffness to hydraulic aperture data from Publications I-II has been added to the compilation from Publication III, Figure 23. The general behaviour matches the data presented in the compilation by Fransson (2009), see Figure 14. That particular data set contains measurements from underground research laboratories in crystalline rock, situated in Canada, Gothenburg and Luleå in Sweden, Äspö HRL and the surficial limestone laboratory in Coaraze, France.

Fransson (2009) compares her data compilation with the trend of stiffness (from storativity) to hydraulic aperture, evaluated from interference tests conducted at Äspö HRL and the adjacent area Laxemar (Rhén et al. 2008) (see eq 29 and section 2.6). In interference tests, the hydraulic response is dominated by the largest fracture in the tested interval. The same trend lines, plus/minus one order of magnitude, are included in Figure 23. The figure consists of two main parts: the stiffness to hydraulic aperture relationship and a conceptual description of fracture

aperture geometries where (a) is a mated fracture, (c) an unmated fracture and (b) an intermediate of (a) and (c). The small colour image represent the aperture distribution (mechanical) of PS0039061, having few contact points. The small grayscale image represents the surface geometry of a fracture sheared under high compressive stress (cf. M in equation 29) this is an example of increased permanent deformation, marked by the upward arrow. The leftward arrow in the diagram is intended to mark the impact of soft fracture filling: reducing b to greater extent than k_n . Group (a) corresponds to many; (c) to few contact points that grows with increased load, giving an increased stiffness but no significant effect on tortuosity since no significant amount of new contacts are generated. Group (b) corresponds to a case where new contact points arise, which increases the tortuosity and reduces the hydraulic aperture, while stiffness is gained.

If the tested borehole has been core-drilled and/or photographed (e.g. BIPS), some information is available on the type of fractures in the borehole. Combined with accurate flow logging of individual fractures (e.g. PFL) the most transmissive fracture of a borehole interval can be identified. However, neither characterisation nor interference tests identify the type of deformation that occurs during a test.

The data from Hallandsås (unfilled hexagons in Figure 23) represent a heavily fractured and conductive rock mass under low stresses. The data fit the trends but most points in this dataset have hydraulic apertures that are calculated to be within the 300-450 μm range. This includes leakage from the injection borehole and thus represents an overestimation. The points are therefore simply plotted on the 300 μm boundary of the diagram in Figure 23. For this reason, only the k_n^a -data is included from Hallandsås, since they are less sensitive to error in the estimation of hydraulic aperture.

The in situ experiments from TASO are represented by filled and unfilled stars in Figure 23. The fracture tested in experiment II had a hydraulic aperture of 130 μm and a stiffness of 40 GPa/m from both changed hydraulic aperture and measured deformation. The other two tests through which it was possible to obtain data do not concur with the general trend; possibly both are influenced by the EDZ and the vicinity to the deformation zone. Test A was at 1.0-1.6 m in KO0014G01 ($b = 3 \mu\text{m}$) and the fracture of focus was horizontal, situated at 1.4 m identified from core mapping and previous hydraulic responses. The core was mapped as unbroken, with no identified mineral filling (Sicada 2013). Test B was at 0.35-0.55 m in the same borehole ($b = 16 \mu\text{m}$). The fracture of focus was at 0.4 m, mapped as broken, and without mineral filling (Sicada 2013). This fracture is well within the prominent

EDZ present in the topmost metre of the boreholes. A general conclusion is that mechanical and hydraulic deformations were small, and modeling indicates similar results (Publication II).

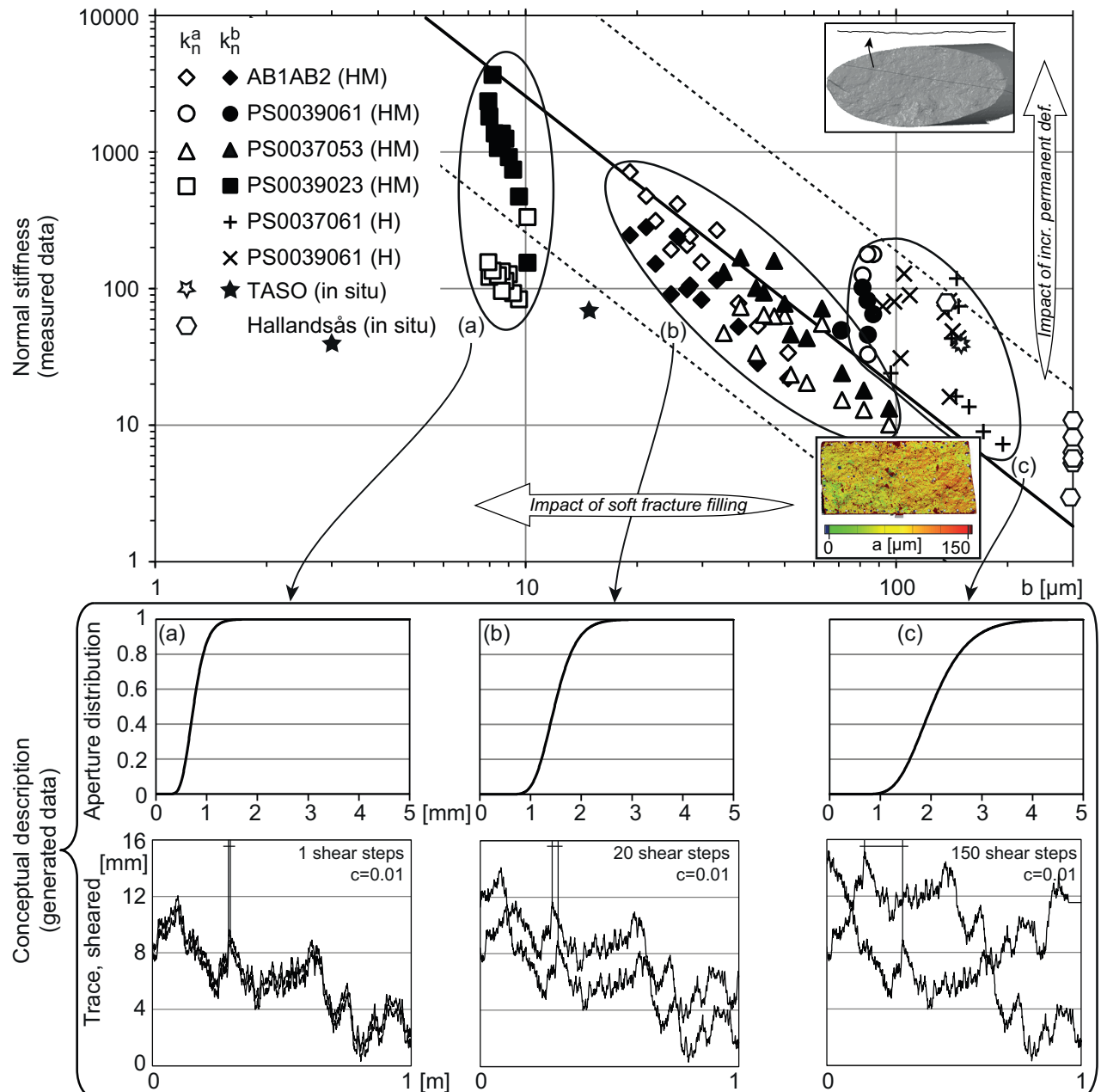


Figure 23 Top half: The results of in situ and laboratory experiments; stiffness plotted against hydraulic aperture. The Hallandsås data has been added on the 300 μm boundary due to a leakage, see text. Bottom half: a conceptual description of fracture aperture geometries presented in Publication III where (a) is a mated fracture, (c) an unmated fracture and (b) an intermediate of (a) and (c). The small colour image represents the aperture distribution (mechanical) of PS0039061, being unmated and having few contact points.

The laboratory results mostly followed the fracture stiffness to hydraulic aperture relationship within plus/minus one order of magnitude, as suggested by Fransson (2009). The relationship is expected to be valid for fractures with limited infilling under low effective compressive stress and small amounts of permanent deformation.

The sample that deviated most from the relationship was PS0039023, which had the lowest aperture among the samples, and was partially sealed. The fact that PS0039023 was partially sealed during the testing implies that it was not reactivated by tunnel excavation or subsequent sampling and processing. The open part of it is therefore tested in stresses about one order of magnitude lower than the pre-excavation stresses since the fracture has been prevented from undergoing substantial shear motion during excavation and sampling. Stiffness from deformation of this sample is not as high as the stiffness from hydraulic aperture, which supports the notion that the fracture had soft infilling that has sealed it partly but did not affect the mechanical normal stiffness to any great extent.

Samples PS0039061 and PS0037061 bend upwards in the graph, showing similarities with the conceptual description c of aperture, with increasing stiffness but limited change of hydraulic aperture. AB1AB2 and PS0037053 follow the conceptual description b, where the stiffness increase coincide with obstruction of flow paths.

Moving from a real fracture in situ to a laboratory-scale sample is not a minor matter. Laboratory samples PS0037053 and PS0037061, for example, were taken from the same fracture, in adjacent slabs, although they behaved differently in the experiments. One explanation for this could be that the contact points supporting the fracture in situ are not sufficiently close to support the 100 by 190 mm samples. The natural variability of the fracture geometry is also likely to influence this behaviour. Small, handling-related dislocations are another, perhaps more plausible explanation.

5.2.2 Hydraulic stiffness-mechanical stiffness relationship

The relationship between stiffness from hydraulic and mechanical deformation of the laboratory experiments is presented in Figure 24. The cross-plot is analogous to a $\Delta a / \Delta b$ ratio since the other component in the equations used for stiffness evaluation is the same for both.

Olsson and Barton (2001) present a data compilation (from Barton (1982) and Barton and de Quadros (1997)) that contains the relationship between mechanical aperture and hydraulic aperture, or mechanical/hydraulic deformations from various

published experiments. PS0039061 and AB1AB2 could fit this description, while PS0037053 and PS0039023 do not.

AB1AB2 is gaining more mechanical stiffness than hydraulic stiffness, see Figure 23 where AB1AB2 is described as gaining contact points and tortuosity, the new contact area is what is slightly dominating. Sample PS0039023 is in the other end of the plot in Figure 24; gaining more hydraulic stiffness than mechanical stiffness, due to a small aperture close to a residual value that is unaffected in the stress range of the experiments.

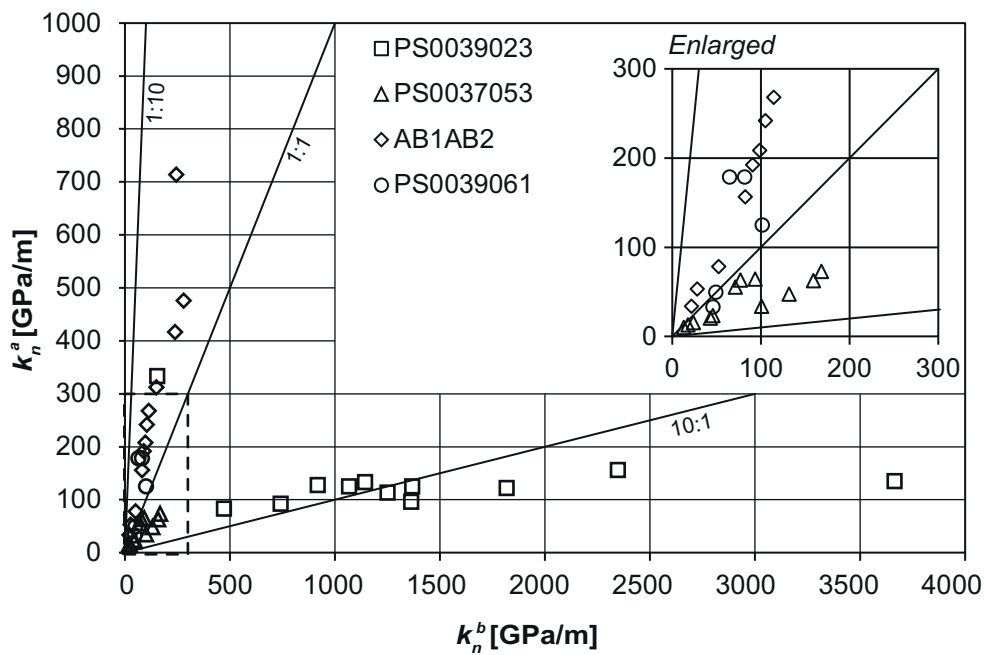


Figure 24 Cross-plot of stiffness from hydraulic and mechanical deformation. The behaviour of different samples varies significantly.

6 CONCLUSIONS

The work conducted in this thesis shows a development towards assessing mechanical properties from hydraulic tests, which would be beneficial in tunnel construction. An example could be to evaluate fracture stiffness from hydraulic testing and use it as input for a rock mechanics design according to an active design scheme, such as the observational method.

Modelling of HM and THM processes (see e.g. Hökmark et al. 2006, 2010; Rutqvist and Stephansson 2003; Rutqvist et al. 2008) relies on assigning appropriate values for parameters such as stiffness. The work conducted here could help to narrow the span of input data and improve the assigning of set-specific properties. This could be a step towards an increased accordance between descriptions of hydromechanical and geomechanical fracture behaviour. With a focus on fracture geometry as a result of geological stress history, more reasonable parameters could be selected.

The in situ measurements in Publication I identified low stiffness in the low-stress and high fracture intensity Hallandsås rock mass. Permanent and resilient deformations were measured in Hallandsås, suggesting that both normal and shear deformations occurred. Measurements in the high-stress, low fracture intensity rock mass in the floor of TASO, Äspö HRL (Publication II) revealed cases with no deformation as well as deformations of a few micrometres.

In Publication III, hydraulic aperture variation of individual fractures was linked to mechanical aperture variation through stiffness for the normal stress range 0 - 2.5 MPa.

The general outcome of the investigations covered in this thesis can be summarised as:

- The results support the hypothesis that a large-aperture fracture has a low fracture normal stiffness, while a smaller aperture may correspond to a high normal stiffness. This is expected to be particularly true for fractures that have undergone translation and compression under low stress.
- Fracture stiffness evaluated from the tests and the stiffness relationship with hydraulic aperture were found to follow the trends linked to the storativity of fractures in Fransson (2009).
- The geological history, including stress history, fracture orientations, shearing and mineral precipitates, affect the hydromechanical behaviour of samples

differently, which is visible in the graphs showing stiffness/aperture (Figure 23) and normal stress/hydraulic aperture/mechanical aperture (Figure 20).

- The previously known hysteretic behaviour of cyclic hydromechanical testing is captured in the experiments.
- The sampling method and the laboratory experimental set-up that were developed were found to be robust.

6.1 Further work

An extended analysis of the fracture surface geometries would be useful to link to different geological signatures (i.e. orientation, stress history and infillings) of individual fractures and their hydromechanical behaviour. This includes topography measurements, providing statistical aperture distributions, as well as the opportunity to look for kinematics. More samples from different fracture sets would be beneficial.

A review and comparison with other available rock mechanical or hydrogeological in situ and lab data from Äspö HRL could enlarge the data sets and strengthen the ideas presented here.

Extending the work to cover fracture zones would be beneficial for understanding larger, potentially complex structures.

Further investigations on how the stress field and fracture orientations affect deformation behaviour and transmissivity would be beneficial.

An integration of hydraulic in-situ testing, fracture topography measurements, statistical aperture distributions and hydromechanical laboratory testing (and/or modelling) would further develop our ability to understand differences between field and laboratory data.

REFERENCES

- Ask D (2004) *New developments of the integrated stress determination method and application to the Äspö Hard Rock Laboratory, Sweden*. PhD Thesis, Royal Institute of Technology, Stockholm, Sweden
- Bandis SC, Lumsden AC, Barton NR (1983) Fundamentals of rock joint deformation. *International Journal of Rock Mechanics and Mining Sciences & Geomechanics Abstracts* 20 (6):249-268
- Barton N (1973) Review of a new shear-strength criterion for rock joints. *Engineering Geology* 7 (4):287-332.
- Barton N (1982) Modelling rock joint behavior from in situ block tests: implications for nuclear waste repository design.
- Barton N, Bandis S, Bakhtar K (1985) Strength, deformation and conductivity coupling of rock joints. *International Journal of Rock Mechanics and Mining Sciences & Geomechanics Abstracts* 22 (3):121-140.
- Barton N, Choubey V (1977) The shear strength of rock joints in theory and practice. *Rock Mechanics* (10):1-54
- Barton N, de Quadros EF (1997) Joint aperture and roughness in the prediction of flow and groutability of rock masses. *International Journal of Rock Mechanics and Mining Sciences* 34 (3-4)
- Bluhm J, Boer R (1996) Effective stresses — a clarification. *Archive of Applied Mechanics* 66 (7):479-492.
- Brown S, Scholz C (1985) Broad Bandwidth Study of the Topography of Natural Rock Surfaces. *Journal of Geophysical Research* 90(B14):12575-12582.
- Brown SR (1995a) Measuring the Dimension of Self-Affine Fractals: Example of Rough Surfaces. In: Barton CC, La Pointe PR (eds) *Fractals in the Earth Sciences*. Plenum Press, New York,
- Brown SR (1995b) Simple mathematical model of a rough fracture. *Journal of Geophysical Research* 100(B4):5941-5952
- Cederbom C, Larson SÅ, Tullborg E-L, Stiberg J-P (2000) Fission track thermochronology applied to Phanerozoic thermotectonic events in central and southern Sweden. *Tectonophysics* 316 (1-2):153-167.
- Darcy H (1856) *Les fontaines publiques de la ville de Dijon*. Dalmont, Paris
- Dershowitz W, Herda HH (1992) Interpretation of fracture spacing and intensity. Paper presented at the 33rd US Symposium on Rock Mechanics,

- Doe TW, Geier JE (1990) *Interpretations of Fracture System Geometry Using Well Test Data, SKB Stripa Project TR 91-03*. Swedish Nuclear Fuel and Waste Management Co, Stockholm, Sweden
- Drake H, Tullborg E-L (2009) *Fracture mineralogy Laxemar: Site descriptive modelling, SDM-Site Laxemar R-08-99*. Swedish Nuclear Fuel and Waste Management Co, Stockholm, Sweden
- Ericsson LO, Brinkhoff P, Gustafson G, Kvartsberg S (2009) *Hydraulic Features of the Excavation Disturbed Zone - Laboratory investigations of samples taken from the Q- and S-tunnels at Äspö HRL. R-09-45*. Swedish Nuclear Fuel and Waste Management Co, Stockholm, Sweden
- Evans KF, Kohl T, Hopkirk RJ, Rybach L (1992) *Modeling of energy production from hot dry rock systems*. Proj Rep Eidgenössische Technische Hochschule (ETH). Zurich, Switzerland
- Fardin N (2001) *Scale dependency, heterogeneity and anisotropy of surface roughness of rock fractures*. PhD Thesis, Royal Institute of Technology, Stockholm, Sweden
- Fardin N, Stephansson O, Jing L (2001) The scale dependence of rock joint surface roughness. *International Journal of Rock Mechanics and Mining Sciences* 38 (5):659-669.
- Faulkner DR, Jackson CAL, Lunn RJ, Schlische RW, Shipton ZK, Wibberley CAJ, Withjack MO (2010) A review of recent developments concerning the structure, mechanics and fluid flow properties of fault zones. *Journal of Structural Geology* 32 (11):1557-1575.
- Fetter CW (2001) *Applied hydrogeology*. Prentice Hall, Upper Saddle River
- Fransson, Tsang CF, Rutqvist J, Gustafson G (2010) Estimation of deformation and stiffness of fractures close to tunnels using data from single-hole hydraulic testing and grouting. *International Journal of Rock Mechanics and Mining Sciences* 47 (6):887-893.
- Fransson Å (2009) *Literature survey: Relations between stress change, deformation and transmissivity for fractures and deformation zones based on in situ investigations. R-09-13*. Swedish Nuclear Fuel and Waste Management Co, Stockholm, Sweden
- Fransson Å, Tsang CF, Rutqvist J, Gustafson G (2007) A new parameter to assess hydromechanical effects in single-hole hydraulic testing and grouting. *International Journal of Rock Mechanics and Mining Sciences* 44 (7):1011-1021.
- Fujifilm (2010) Prescale. <http://www.fujifilm.com/products/prescale/prescalefilm/>. Accessed 2010-10-26

- Gentier S, Billiaux D, van Vliet L (1989) Laboratory testing of the voids of a fracture. *Rock Mechanics and Rock Engineering* 22 (2):149-157.
- Goodman RE (1970) Deformability of joints. Paper presented at the *Symposium for Determination of the In-Situ Modulus of Deformation of Rock.*, Denver, Colorado,
- Goodman RE (1974) The mechanical properties of joints. In: *Proceedings of the 3rd Int. Congr. International Society of Rock Mechanics*, Denver, Colorado, 1974. National Academy of Sciences, Washington, DC, pp 127–140
- Goodman RE (1976) *Methods of geological engineering in discontinuous rocks*. West, St. Paul, Minn.
- Gustafson G (2012) *Hydrogeology for Rock Engineers*. BeFo, Stockholm, Sweden
- Hakala M, Kempainen K, Siren T, Heine J, Christiansson R, Martin CD, Koskinen T (2012) Experience with a new LVDT-Cell to measure in-situ stress from an existing tunnel. Paper presented at *Eurock2012*, Stockholm, Sweden,
- Hakami E (1988) *Water flow in single rock joints*. Licentiate Thesis. Luleå University of Technology, Luleå
- Hakami E (1995) *Aperture distribution of rock fractures*. PhD Thesis, Royal Institute of Technology, Stockholm, Sweden
- Hakami E, Barton N Aperture measurements and flow experiments using transparent replicas of rock joints. In: Stephansson O, Barton N (eds) *Rock joints : proceedings of the International Symposium on Rock Joints*, Loen / Norway / 4-6 June 1990, Loen/Norway, 1990. Balkema,
- Hakami E, Hakami H, Cosgrove J (2002) *Strategy for a Rock Mechanics Site Descriptive Model. Development and testing of an approach to modelling the state of stress*. SKB R-02-03. Swedish Nuclear Fuel and Waste Management Co, Stockholm, Sweden
- Hakami E, Larsson E (1996) Aperture measurements and flow experiments on a single natural fracture. *International Journal of Rock Mechanics and Mining Sciences & Geomechanics Abstracts* 33 (4):395-404.
- Heiland J (2003) Laboratory testing of coupled hydro-mechanical processes during rock deformation. *Hydrogeology Journal* 11 (1):122-141.
- Hernqvist L (2009) *Characterization of the Fracture System in Hard Rock for Tunnel Grouting*. Licentiate Thesis, Chalmers University of Technology, Gothenburg, Sweden
- Hökmark H, Fälth B, Wallroth T (2006) *T-H-M couplings in rock: overview of results of importance to the SR-Can safety assessment*. SKB R-06-88. Swedish Nuclear Fuel and Waste Management Co, Stockholm, Sweden

- Hökmark H, Lönnqvist M, Fälth B (2010) *THM-issues in repository rock. Thermal, mechanical, thermo-mechanical and hydro-mechanical evolution of the rock at the Forsmark and Laxemar sites. SKB TR-10-23*. Swedish Nuclear Fuel and Waste Management Co, Stockholm, Sweden
- Iwano M (1995) *Hydromechanical Characteristics of a Single Rock Joint*. PhD Thesis. Massachusetts Institute of Technology, MA, USA
- Jaeger JC, Cook NGW (1969) *Fundamentals of rock mechanics*. London
- Janson T, Stigsson M (2002) *Test with different stress measurement methods in two orthogonal bore holes in Äspö HRL. SKB R-02-26*. Swedish Nuclear Fuel and Waste Management Co, Stockholm, Sweden
- Jing L, Stephansson O (2007) Fluid Flow and Coupled Hydro-Mechanical Behavior of Rock Fractures. In: Lanru J, Ove S (eds) *Developments in Geotechnical Engineering*, vol Volume 85. Elsevier, pp 111-144.
- Kirsch G (1898) Die Theorie der Elastizität und die Bedürfnisse der Festigkeitslehre. *Veit Deut Ing* 42 (28):797-807
- Kranz RL, Frankel AD, Engelder T, Scholz CH (1979) The permeability of whole and jointed Barre Granite. *International Journal of Rock Mechanics and Mining Sciences and Geomechanical Abstracts* 16 (4):225-234
- Kvartsberg S, Mossmark F, Fransson Å ((submitted)) Early engineering geological prognosis of grouting design prerequisites: an approach applied to the Hallandsås project in Sweden. *Engineering Geology*
- Labuz J, Zang A (2012) Mohr–Coulomb Failure Criterion. *Rock Mechanics and Rock Engineering* 45 (6):975-979.
- Lanaro F (2001) *Geometry, mechanics and transmissivity of rock fractures*. PhD Thesis. Royal Institute of Technology, Stockholm, Sweden
- Larsson E (1997) *Groundwater flow through a natural fracture -flow experiments and numerical modelling*. Licentiate Thesis. Chalmers University of Technology, Gothenburg, Sweden
- Larsson S-Å, Tullborg E-L (1993) *Tectonic Regimes in the Baltic Shield during the last 1200 Ma -A review. SKB TR-94-05*. Swedish Nuclear Fuel and Waste Management Co, Stockholm, Sweden
- Legrain H, Tshibangu JP (2006) Roughness characterization of rock fractures surfaces. In: *Eurock 2006: Multiphysics Coupling and Long Term Behaviour in Rock Mechanics*, Taylor & Francis, pp 591-596.
- Lindblom U (2010) *Bergbyggnad*. Liber, Gothenburg, Sweden
- Ljunggren C, Chang Y, Janson T, Christiansson R (2003) An overview of rock stress measurement methods. *International Journal of Rock Mechanics and Mining Sciences* 40 (7–8):975-989.

- Munier R (1993) *Segmentation, fragmentation and jostling of the Baltic shield with time*. PhD Thesis Faculty of Science,37. University of Uppsala, Sweden
- Munier R (1995) *Studies of Geological Structures at Äspö: Comprehensive Summary of Results. Äspölaboratoriet Progress Report, vol 25-95-21*. Swedish Nuclear Fuel and Waste Management Co, Stockholm, Sweden
- Munier R, Stenberg L, Stanfors R, Milnes AG, Hermanson J, Triumf C-A (2003) *Geological Site Descriptive Model. A strategy for the model development during site investigations. SKB R-03-07*. Swedish Nuclear Fuel and Waste Management Co, Stockholm, Sweden
- Nemoto K, Watanabe N, Hirano N, Tsuchiya N (2009) Direct measurement of contact area and stress dependence of anisotropic flow through rock fracture with heterogeneous aperture distribution. *Earth and Planetary Science Letters* 281 (1-2):81-87.
- NRC (1996) *Rock fractures and fluid flow : contemporary understanding and applications*. National Academy, Washington, D.C.
- Olofsson B (1991) *Impact on groundwater conditions by tunnelling in hard crystalline rocks*. PhD Thesis. Royal Institute of Technology, Stockholm, Sweden
- Olsson R (1997) *The Effective Stress Concept in a Jointed Rock Mass*. Report B 1997:3. Department of Geotechnics, Chalmers University of Technology,
- Olsson R (1998) *Mechanical and hydromechanical behaviour of hard rock joints a laboratory study*. Ph.D. Thesis, Chalmers University of Technology, Gothenburg, Sweden
- Olsson R, Barton N (2001) An improved model for hydromechanical coupling during shearing of rock joints. *International Journal of Rock Mechanics and Mining Sciences* 38 (3):317-329.
- Power WL, Durham WB (1997) Topography of natural and artificial fractures in granitic rocks: Implications for studies of rock friction and fluid migration. *International Journal of Rock Mechanics and Mining Sciences* 34 (6):979-989.
- Pyrak-Nolte LJ, Myer LR, Cook NGW, Witherspoon PA (1987) Hydraulic and Mechanical Properties of Natural Fractures in Low Permeability Rock. Paper presented at the *Sixth International Congress on Rock Mechanics*, Montreal, Canada, August 1987
- Rawnsley KD, Rives T, Petti JP, Hencher SR, Lumsden AC (1992) Joint development in perturbed stress fields near faults. *Journal of Structural Geology* 14 (8-9):939-951.
- Rhén I, Forsmark T, Hartley L, Jackson P, Roberts D, Swan D, Gylling B (2008) *Hydrogeological conceptualisation and parameterisation, Site descriptive*

- modelling SDM–Site Laxemar. R-08-78.* Swedish Nuclear Fuel and Waste Management Co, Stockholm, Sweden
- Rocscience (2010) *Examine 2D*. 7 edn. www.rocscience.com, Toronto, Canada
- Rosberg J-E (2010) *Well testing, methods and applicability*. PhD Thesis. Engineering Geology, Lund University, Lund, Sweden
- Runslätt E, Thörn J (2010) *Fracture deformation when grouting in hard rock: In situ measurements in tunnels under Gothenburg and Hallandsås*. MSc. Thesis, Chalmers University of Technology, Gothenburg
- Rutqvist J, Birkholzer JT, Tsang C-F (2008) Coupled reservoir–geomechanical analysis of the potential for tensile and shear failure associated with CO₂ injection in multilayered reservoir–caprock systems. *International Journal of Rock Mechanics and Mining Sciences* 45 (2):132-143.
- Rutqvist J, Stephansson O (2003) The role of hydromechanical coupling in fractured rock engineering. *Hydrogeology Journal* 11 (1):7-40.
- Sicada (2013) Data delivery Sicada_13_038. Swedish Nuclear Fuel and Waste Management Co, Stockholm, Sweden
- SKB (2011) *Long-term safety for the final repository for spent nuclear fuel at Forsmark: Main report of the SR-Site project TR-11-01*. Swedish Nuclear Fuel and Waste Management Co, Stockholm, Sweden
- Snow DT (1968) Rock fracture spacings, openings and porosities. *Proc Amer Soc Civil Engineers* 94(SM1):73-79
- SOU (1998) *Kring Hallandsåsen: delrapport från Tunnelkommissionen*. Statens offentliga utredningar, 0375-250X ; 1998:60. Fritzes offentliga publikationer, Stockholm
- Staub I, Andersson C, Magnor B (2004) *Äspö Pillar Stability Experiment. Geology and mechanical properties of the rock in TASQ SKB R-04-01*. Swedish Nuclear Fuel and Waste Management Co, Stockholm, Sweden
- Stephansson O, Dahlström L-O, Bergström K, Myrvang A, Fjeld OK, Hanssen TH, Särkkä P, Väättäinen A (1987) *Fennoscandian Rock Stress Data Base - FRSDB. Forskningsrapport / Luleå University of Technology 1987:06*. Luleå, Sweden
- Stephansson O, Ljunggren C, Jing L (1991) Stress measurements and tectonic implications for Fennoscandia. *Tectonophysics* 189 (1–4):317-322.
- Stephens M, Wahlgren C-H, Söderbäck Be (2008) *Geological evolution, palaeoclimate and historical development of the Forsmark and Laxemar-Simpevarp areas. Site descriptive modelling, SDM-Site. SKB R-08-19*. Swedish Nuclear Fuel and Waste Management Co, Stockholm, Sweden

- Sturk R, Dudouit F, Aurell O, Eriksson S (2011) Summary of the First TBM Drive at the Hallandsås Project. Paper presented at the 2011 *Rapid Excavation and Tunneling Conference*
- Talbot CJ, Sirat M (2001) Stress control of hydraulic conductivity in fracture-saturated Swedish bedrock. *Engineering Geology* 61 (2-3):145-153.
- Tatone BSA, Grasselli G (2009) A method to evaluate the three-dimensional roughness of fracture surfaces in brittle geomaterials. *Review of Scientific Instruments* 80 (12):125110-125110.
- Tatone BSA, Grasselli G (2010) A new 2D discontinuity roughness parameter and its correlation with JRC. *International Journal of Rock Mechanics and Mining Sciences* 47 (8):1391-1400.
- Terzaghi K The shear resistance of saturated soils. In: Proceedings for the *1st. International Conference on Soil Mechanics and Foundation Engineering*, Cambridge, MA, 1936. pp 54-56
- Thörn J (2012) *Coupling between changes in hydraulic and mechanical aperture: A laboratory study on rock cores. Report 2012:9*. Chalmers University of Technology, Gothenburg
- Wang HF (2000) *Theory of linear poroelasticity : with applications to geomechanics and hydrogeology*. Princeton series in geophysics. Princeton University Press, Princeton, N.J.
- Wass E, Nyberg G (2009) *Äspö Hard Rock Laboratory. Hydro Monitoring Program. Report for 2009. SKB IPR-10-08*. Swedish Nuclear Fuel and Waste Management Co, Stockholm, Sweden
- Wastenson L, Fredén C (2002) *Sveriges nationalatlas. Berg och jord [Kartografiskt material]*. Sveriges nationalatlas (SNA), Vällingby :
- Witherspoon PA, Wang JSY, Iwai K, Gale JE (1980) Validity of the cubic law for fluid flow in a deformable fracture. *Water Resources Research* 16 (6):1016-1024.
- Zangerl C, Evans KF, Eberhardt E, Loew S (2008) Normal stiffness of fractures in granitic rock: A compilation of laboratory and in-situ experiments. *International Journal of Rock Mechanics and Mining Sciences* 45 (8):1500-1507.
- Zimmerman R, Main I (2003) Chapter 7 Hydromechanical Behavior of Fractured Rocks. In: Yves G, Maurice B (eds) *International Geophysics*, vol Volume 89. Academic Press, pp 363-421
- Zimmerman RW, Bodvarsson GS (1996) Hydraulic conductivity of rock fractures. *Transport in Porous Media* 23 (1):1-30.

